Quaternary Science Reviews 192 (2018) 27–46

Contents lists available at ScienceDirect

Quaternary Science Reviews

journal homepage: www.elsevier.com/locate/quascirev

Invited review

Beyond the bipolar seesaw: Toward a process understanding of interhemispheric coupling

Joel B. Pedro [a, *], Markus Jochum [a], Christo Buizert [b], Feng He [c, b], Stephen Barker [d], Sune O. Rasmussen [a]

[a] Center for Ice and Climate, Niels Bohr Institute, University of Copenhagen, Copenhagen, Denmark
[b] College of Earth, Ocean, and Atmospheric Sciences, Oregon State University, Corvallis, OR, USA
[c] Center for Climatic Research, Nelson Institute for Environmental Studies, University of Wisconsin-Madison, Madison, WI, USA
[d] School of Earth and Ocean Sciences, Cardiff University, Cardiff, UK

ARTICLE INFO

Article history:
Received 12 December 2017
Received in revised form
3 May 2018
Accepted 3 May 2018

Keywords:
Bipolar ocean seesaw
Atlantic Meridional Overturning Circulation
Millennial-scale climate variability
Dansgaard–oeschger event
Antarctic Isotope Maximum
Sea ice
Southern Ocean
Antarctic Circumpolar Current

ABSTRACT

The thermal bipolar ocean seesaw hypothesis was advanced by Stocker and Johnsen (2003) as the 'simplest possible thermodynamic model' to explain the time relationship between Dansgaard–Oeschger (DO) and Antarctic Isotope Maxima (AIM) events. In this review we combine palaeoclimate observations, theory and general circulation model experiments to advance from the conceptual model toward a process understanding of interhemispheric coupling and the forcing of AIM events. We present four main results: (1) Changes in Atlantic heat transport invoked by the thermal seesaw are partially compensated by opposing changes in heat transport by the global atmosphere and Pacific Ocean. This compensation is an integral part of interhemispheric coupling, with a major influence on the global pattern of climate anomalies. (2) We support the role of a heat reservoir in interhemispheric coupling but argue that its location is the global interior ocean to the north of the Antarctic Circumpolar Current (ACC), not the commonly assumed Southern Ocean. (3) Energy budget analysis indicates that the process driving Antarctic warming during AIM events is an increase in poleward atmospheric heat and moisture transport following sea ice retreat and surface warming over the Southern Ocean. (4) The Antarctic sea ice retreat is itself driven by eddy-heat fluxes across the ACC, amplified by sea-ice–albedo feedbacks. The lag of Antarctic warming after AMOC collapse reflects the time required for heat to accumulate in the ocean interior north of the ACC (predominantly the upper 1500 m), before it can be mixed across this dynamic barrier by eddies.

1. Introduction

The thermal bipolar ocean seesaw hypothesis is the prevailing explanation for the coupling of Dansgaard–Oeschger (DO) and Antarctic Isotope Maxima (AIM) events. Stocker and Johnsen (2003) provide the thermodynamic basis for the hypothesis with their suggestion that the temperature anomalies in Greenland and Antarctica during these events could most simply be explained by changes in the rate of cross-equatorial ocean heat transport in the Atlantic, that are modulated at southern high latitudes by a large heat reservoir (commonly assumed to be the Southern Ocean). While the simplicity of the thermal seesaw hypothesis is attractive, the absence of details on the actual physical processes that connect north and south limits its application to the coupled climate system (Wunsch, 2006; Seager and Battisti, 2007; Clement and Peterson, 2008). Indeed, Stocker & Johnsen (2003) did not intend that their conceptual model captured all the relevant physics. The purpose of this review is to explore several key limitations of the thermal seesaw: the means of signal transmission in the Atlantic, the location and means of operation of the heat reservoir, signal propagation across the Antarctic Circumpolar Current and the forcing of Antarctic temperature itself.

The paper is structured as follows: The remainder of Section 1 outlines the development of the thermal seesaw hypothesis and several of its limitations; Section 2 introduces two transient global climate model (GCM) experiments that we use, along with palaeoclimate data, to explore these limitations; Section 3 presents our results on ocean, atmospheric and radiative processes responsible

* Corresponding author.
E-mail address: jpedro@nbi.ku.dk (J.B. Pedro).

https://doi.org/10.1016/j.quascirev.2018.05.005
0277-3791/

for transmission of temperature anomalies between the northern and southern high latitudes; Section 4 describes an energy budget analysis of the specific processes driving Antarctic warming and cooling; Section 5 compares our results to several major predictions and assumption of the thermal seesaw; we conclude in Section 6 with some suggestions on future lines of research that would aid further understanding of the mechanisms involved in interhemispheric coupling and the forcing of AIM events in particular.

1.1. Origin of the thermal seesaw hypothesis

Greenland ice-core records spanning the last glacial period and deglaciation feature abrupt Dansgaard–Oeschger temperature variations of 10–16 °C, between cold (Greenland stadial) and warmer (Greenland interstadial) climate states, see Fig. 1a (Severinghaus et al. 1998; Huber et al. 2006; Kindler et al. 2014). Antarctic ice cores feature smaller and more gradual temperature variation of 1–3 °C amplitude, termed Antarctic Isotope Maxima, see Fig. 1b (EPICA Community Members, 2006; Stenni et al. 2011; Parrenin et al. 2013; WAIS Divide Project Members, 2015). The thermal seesaw concept emerged by heuristically connecting the timing and shape of the DO and AIM events with theory on ocean heat transport and observations of palaeocean circulation (Mix et al. 1986; Crowley, 1992; Stocker and Johnsen, 2003). We briefly review each of these building blocks of the thermal seesaw.

Analysis of the relative timing of the DO and AIM events was made possible by gas-based ice-core synchronisations (Bender et al., 1994), in particular the fast global variations in atmospheric methane that accompany DO transitions (Blunier et al., 1998; Blunier and Brook, 2001). The North Greenland Ice Core Project (NGRIP) and multi-core Antarctic temperature reconstruction shown in Fig. 1 are aligned using this technique. The ice-core data suggest a systematic relationship: Antarctica gradually warms during Greenland stadials (Fig. 1 shading), and gradually cools during Greenland interstadials (Blunier et al., 1998; Blunier and Brook, 2001; EPICA Community Members, 2006; Pedro et al. 2011; WAIS Divide Project Members, 2015). Some internal differences between Antarctic ice-core sites in the structure of AIM events have also been identified (and see Landais et al. 2015; Morgan et al. 2002, and our Section 5).

The principle behind the second building block of the thermal seesaw—net northward heat transport in the Atlantic Ocean—was proposed close to 150 years ago by James Croll.

> "The [Atlantic] currents, which cross the equator are far higher in temperature than their compensating undercurrents; consequently there is constant transference of heat from the southern hemisphere to the northern [Croll, 1870]."

Modern observations and reanalysis data confirm that the Atlantic transports heat northward at all latitudes (Ganachaud and Wunsch, 2000; Trenberth and Caron, 2001; Trenberth and Fasullo, 2017). Today, we associate this northward heat transport (around 1±0.5 PW at the equator) with the warm surface flow and cold deep return flow of the Antarctic Meridional Overturning Circulation (AMOC): warm waters flow northward in the Atlantic surface layers, cool and sink in the polar North Atlantic and then return south, mixing with intermediate depth waters, before returning to the surface either by wind-driven isopycnal upwelling in the Southern Ocean (Toggweiler and Samuels, 1995; Munk and Wunsch, 1998; Marshall and Speer, 2012) or by diapycnal diffusion in the Indo-Pacific basins (Talley, 2013).

The potential for instability of the ocean overturning circulation, with major consequences for the climate system, was first pointed out by Stommel (1961), whose simple density-driven model of overturning circulation suggested that small changes in salt or heat inputs could tip the circulation into an alternative stable regime. Crowley (1992) argued that a collapse of the AMOC would warm

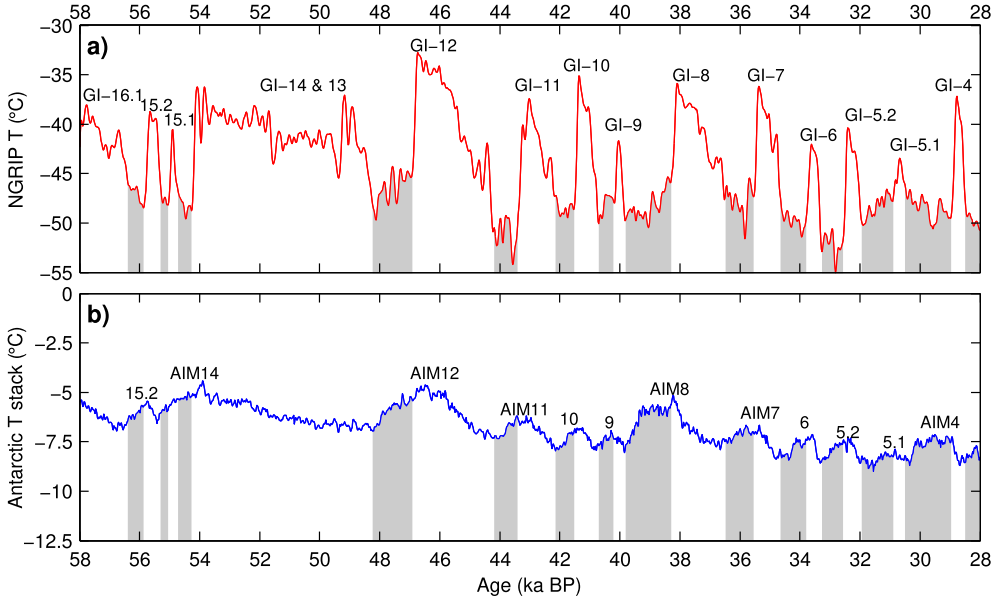

Fig. 1. Temperature reconstructions from Greenland and Antarctic ice cores spanning Marine Isotope Stage 3. a) North Greenland Ice Core Project (NGRIP) temperature reconstruction based on δ^{15}N and δ^{18}O records (North Greenland Ice Core Project members, 2004; Kindler et al., 2014). b) Antarctic Temperature Stack (ATS) based on stacked δ^{18}O and δD records from six Antarctic ice cores: EPICA Dome C, EPICA Dronning Maud Land (EDML), Vostok, Talos Dome, and Dome Fuji as published in (Parrenin et al., 2013), to which we have added data from the WAIS Divide Core (Cuffey et al., 2016). Note how the warming phases of Antarctic Isotope Maxima (AIM) coincide with Greenland stadials (GS; grey shading) and the cooling phase of AIMs coincide with Greenland interstadials (GI). The AIM labelling follows EPICA Community Members (2006) and the GI and GS labeling follows Rasmussen et al. (2014). The time axis is given in thousand of years before 1950 AD, on the Antarctic Ice Core Chronology 2012 (AICC 2012) timescale of Veres et al. (2013). Antarctic temperatures are expressed as an anomaly with respect to the past millennium. Note the much larger temperature variations in Greenland compared to Antarctica and the different ranges of their respective temperature axes.

the South Atlantic at the same time as cooling the North Atlantic due to a change in heat advection: i.e. heat which the surface flow would otherwise have exported north would be left to accumulate in the south (and vice versa for a strengthening of the AMOC). This opposing North and South Atlantic surface temperature response to AMOC perturbation was demonstrated in a zonally-averaged ocean–atmosphere model with simplified geometry by Stocker et al. (1992) and is seen in models ranging from intermediate complexity to fully coupled GCMs (e.g. Ganopolski and Rahmstorf, 2001; Schmittner et al., 2003; Peltier and Vettoretti, 2014), with some notable exceptions in which the South Atlantic temperature response is more muted (e.g. Kageyama et al., 2013).

Turning to the palaeoceanographic evidence, rapid shifts in North Atlantic planktic foraminifera assemblages during the abrupt deglacial climate changes in Greenland were found in a high resolution marine sediment core by Ruddiman and McIntyre (1981), and linked by these authors and others to variations in North Atlantic Deep Water production (Broecker et al., 1985; Broecker and Denton, 1989). Subsequent evidence that large-scale changes in Atlantic circulation accompany the DO events has come from a wide range of circulation proxies including seawater Nd isotope ratios (e.g. Piotrowski et al. 2005), benthic foraminiferal $\delta^{13}C$ (e.g. Curry and Oppo, 1997; Shackleton et al. 2000), Cd/Ca ratios (e.g. Adkins et al., 1998), tracers for carbonate chemistry and sedimentary dissolution (B/Ca ratios) (e.g. Barker et al., 2010; Gottschalk et al., 2015), Pa/Th isotope ratios (Henry et al., 2016), variations in sediment magnetic activity and variations in sediment grain size (e.g. Kissel et al. 2008). The weight of evidence from these records suggests that reductions in AMOC strength and in North Atlantic Deep Water production (NADW) coincide with Greenland stadial conditions and AIM warming stages, while increases in AMOC strength and NADW production coincide with Greenland interstadial and AIM cooling stages (see the review by Lynch-Stieglitz, 2017). However, uncertainties in cross-dating ice and marine cores currently prevent a clear answer on whether abrupt changes in the AMOC slightly lag or sightly lead the DO abrupt transitions in Greenland.

Crowley's Atlantic seesaw predicts opposite temperature variations between the North Atlantic and South Atlantic during DO events, which is supported by marine core data (Sachs and Lehman, 1999; Barker et al., 2009). Stocker and Johnsen (2003) build on Crowley's Atlantic seesaw by adding a heat reservoir in the south, commonly assumed to be the Southern Ocean, that gradually accumulates heat when the South Atlantic is warm and gradually loses heat when the South Atlantic is cold. By convolving the South Atlantic temperature anomalies with a slow timescale of heat uptake by the reservoir, their thermal seesaw offers an explanation for the damped and gradual character of the AIM temperature variations in Antarctica. The implicit and testable assumption is that Antarctic temperatures during AIM events monitor the rise and fall of Southern Ocean heat content. The paper also includes an important caveat about the location of the thermal reservoir:

> "the heat reservoir could be the glacial Southern Ocean, but the model is obviously too simple to prove this statement. Other processes and climate system components such as e.g., terrestrial ice sheets, could be responsible for the thermal damping of northern temperature variations" (Stocker and Johnsen, 2003 pp4)".

To our knowledge there has not been any rigorous testing of the location of the heat reservoir or of its means of heat exchange with the South Atlantic. Conducting such tests in the framework of a coupled GCM is one of the objectives of our study.

We would like to emphasise that there is not yet a consensus on the cause of past AMOC variations, possibilities include freshwater release from northern hemisphere ice sheets (e.g. Bond and Lotti, 1995; Ganopolski and Rahmstorf, 2001; Vellinga and Wood, 2002), an internal salt oscillator in the North Atlantic (Broecker et al. 1990; Peltier and Vettoretti, 2014), stochastic atmospheric forcing originating in the tropics (Kleppin et al. 2015; Steffensen et al. 2008; Thomas et al. 2009), the effect of changes in the height of the Laurentide ice sheet on the path of the polar jetstream (Zhang et al. 2014) and variations in atmospheric CO_2(Banderas et al., 2015; Zhang et al., 2017). It's also been suggested that AMOC variability may be a result of DO events rather than their cause, e.g. via abrupt changes in sea ice conditions and stratification in the Nordic and/or Labrador Seas (Dokken et al., 2013; Kleppin et al., 2015). Note that the thermal seesaw hypothesis itself makes no claim about the trigger of AMOC variability; rather it is a theory on the climate response. Hence, for the purpose of this paper we assume that the global expression of DO events is independent of the DO trigger and that DO events are associated with AMOC changes.

The term "bipolar seesaw" has also been used to describe competition between the relative strength of the North Atlantic deep water (NADW) and Antarctic bottom water (AABW) cells of the global ocean overturning (Broecker, 1998). To be clear, our focus in this paper is on evaluating the thermal seesaw mechanism as described by Crowley (1992) and Stocker and Johnsen (2003) and not the 'deep-water seesaw' of Broecker (1998). Evaluations of the deep-water mechanism can be found elsewhere (e.g. Stouffer et al., 2007; Swingedouw et al., 2009; Menviel et al., 2015; Buizert and Schmittner, 2015).

Before concluding this brief introduction to the origins of the thermal seesaw concept, we return to the ice-core data itself. The precise time relationship between the DO and AIM events has been a subject of ongoing debate in the literature (e.g. Blunier et al., 1998; Steig and Alley, 2002; Schmittner et al., 2003; Huybers, 2004). A comprehensive study of this time relationship was recently conducted on the WAIS Divide Core (WDC). WAIS Divide Project Members (2015) stack all NGRIP DO and WDC AIM events (after aligning them using coincident methane variations in the two cores) and show that on average the start of AIM warming events in the WDC core lags the Greenland stadial cooling transition by 208±96 years (2σ uncertainty); similarly the termination of AIM

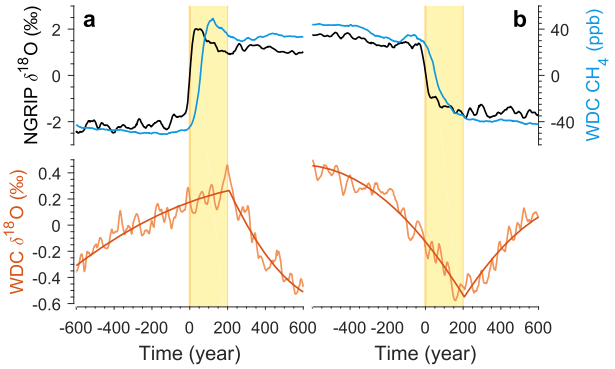

Fig. 2. Time relationships between Greenland and Antarctic ice-core data during Marine Isotope Stage 3. a) Stacked data from DO 3–18 of NGRIP $\delta^{18}O$ (black), WDC methane (blue) and WDC $\delta^{18}O$ (orange curve with fit), aligned at the mid point of the NGRIP interstadial transitions; on average Antarctica begins cooling 218±92 years after each Greenland interstadial warming transition. b) As for a) but for NGRIP stadial transitions; on average Antarctica begins warming 208±96 years after each Greenland stadial cooling transition. The errors denote 95% confidence levels accounting for dating and procedural uncertainties. WDC data is from WAIS Divide Project Members (2015), NGRIP data from North Greenland Ice Core Project members (2004). Figure adapted from WAIS Divide Project Members (2015).

warming trends lags Greenland interstadial warming transitions by on average 218±92 years see (Fig. 2a and b). From this centennial lag, the authors conclude that an oceanic teleconnection couples the high-latitude climates of both hemispheres during the DO events. Based on previous marine sediment core observations (Barker et al. 2009) and theory on signal propagation in the Atlantic (Kawase, 1987), they suggest that the DO signal is rapidly transmitted from the North Atlantic to the South Atlantic, before taking one to two centuries to cross the Antarctic Circumpolar Current into the high-latitude Southern Ocean. This explanation implies that sea surface temperature (SST) to the south of the Antarctic Circumpolar Current is the dominant driver of Antarctic temperature during AIM events, however the mechanisms connecting SST and Antarctic temperature were not specified.

1.2. Challenges and limitations to the thermal seesaw concept

In this section we discuss several aspects of interhemispheric coupling where assumptions implicit in the thermal seesaw have been challenged, and/or where the processes operating in the coupled climate system are beyond the scope of the original conceptual model.

The first challenge concerns the dominance of the atmosphere over the ocean in total poleward heat transport. At mid to high latitudes, poleward atmospheric heat transport exceeds poleward ocean heat transport by an order of magnitude; for example at 40°S over 90% of poleward heat flux is carried by the atmosphere (Trenberth and Caron, 2001). Wunsch (2006) and Seager and Battisti (2007) question the thermal seesaw assumption that the Atlantic Ocean, with its comparatively small portion of heat transport to high latitudes, is likely to be the main player in millennial-scale climate variability. On the other hand it is difficult to argue that DO and AIM coupling could be exclusively an atmospheric phenomena: the intrinsic dynamical processes and teleconnections in the atmosphere typically occur on much shorter timescales, whereas the ocean has the thermal mass to store heat over centuries to millennia.

Wunsch (2006) argues further that changes in cross-equatorial Atlantic Ocean heat transport invoked by the thermal seesaw could be compensated, or even overwhelmed, by the much larger heat transports in the global atmosphere and/or by variations in Pacfic Ocean heat transport. The principle of compensation between meridional energy transport in the ocean and atmosphere was set out by Bjerknes (1964), who suggested that opposite fluctuations in the oceanic and atmospheric components of heat transport in the Atlantic sector are needed to keep the top-of-atmosphere (TOA) radiative budget fixed on long time scales. Partial 'Bjerknes compensation' has since been detected in coupled models of intermediate complexity and in full GCMs (Shaffrey and Sutton, 2004; Farneti and Vallis, 2013; Vettoretti and Peltier, 2018). However, even in the case of perfect compensation, climate anomalies are still expected: e.g. the GCM experiments of Cheng et al. (2007) find that North Atlantic sea ice is much more sensitive to changed ocean heat transport than to an equivalent change in atmospheric heat transport; furthermore, the effect of sea ice change on surface temperature is amplified by additional feedbacks (e.g. albedo, low cloud cover and water vapour).

A second challenge to the thermal seesaw concerns signal propagation in the Atlantic Ocean. The South Atlantic temperature anomaly is commonly assumed to result from changed heat advection: i.e. the AMOC collapses and the heat that is no-longer delivered to the North Atlantic accumulates in the South Atlantic (Crowley, 1992; Seidov and Maslin, 2001). While this is a reasonable conjecture, it implies that the ocean functions like a set of communicating vessels. In a three dimensional coupled system like Earth, however, other responses are possible. More specifically, since much of the return flow of the AMOC passes through the tropical Ekman layer (Jochum and Malanotte-Rizzoli, 2001) a reduced AMOC may heat the equatorial surface waters and release heat to the atmosphere rather than store it in the South Atlantic (see e.g. Liu et al. 1994; Liu and Philander, 1995). A multi-model comparison of AMOC perturbation experiments by Kageyama et al. (2013) found that South Atlantic warming is a common but not ubiquitous response to AMOC collapse, suggesting that there is more to South Atlantic warming than changed advection.

Stocker and Johnsen (2003) do not specify the means of signal propagation in the Atlantic, but note that a fast connection between the North and South Atlantic may be afforded by the vertical displacement of isopycnals associated with wave propagation. Previous modelling studies suggest that density anomalies in the North Atlantic associated with changing deep water formation are propagated on a timescale of months to decades throughout the global ocean by Kelvin and Rossby waves (Kawase, 1987; Huang et al. 2000; Johnson and Marshall, 2002). The waves can generate large temperature anomalies by displacing the thermocline. Kelvin waves travel only along coastal boundaries and the equator. Rossby waves radiate westward from coastal boundaries, propagating the Kelvin wave-driven isopycnal depth adjustments into the ocean interior. Both planetary wave types can also be excited by changes in wind stress.

Schmittner et al. (2003) argue that wave propagation explains the decadal-scale appearance of opposing North and South Atlantic temperature anomalies in AMOC perturbation experiments with the intermediate complexity (UVIC) model. However, their fixed winds and energy-moisture balance atmosphere precludes the operation of atmosphere–ocean interactions, which may also be important in setting South Atlantic thermocline depth and heat storage. Given the strong evidence that migration of the Atlantic ITCZ (and thus of the equatorial trade winds) accompanies DO transitions (Tierney et al. 2008; Mosblech et al. 2012; Cheng et al. 2013), we examine whether wind forcing may also play a role in setting South Atlantic temperature anomalies during DO events (see Section 3.4).

A third challenge concerns the propagation of temperature anomalies between the South Atlantic and Southern Ocean. The thermal seesaw predicts that the strongest South Atlantic temperature anomalies occur within the top 1000 m, the depth range of the AMOC return flow (Stocker and Johnsen, 2003). Signal propagation into the Southern Ocean at these depths is physically inhibited by the dynamic barrier formed by the Antarctic Circumpolar Current (ACC). The ACC can not be crossed at these depths by advection or wave propagation because of the absence of a meridional boundaries (e.g. Cox, 1989; Schmittner et al. 2003). Advective transport across the latitudes of the ACC is only possible along the topographic ridges which occur below ca. 1500 m depth (Toggweiler and Samuels, 1995). Hence, in the upper 1500 m anomaly propagation across the steeply outcropping isopycnals of the ACC must rely on eddy fluxes which are less efficient than wave propagation and advection in signal transmission (McDougall and Church, 1986), thus questioning from a theoretical standpoint whether the Southern Ocean is likely to act as a thermal reservoir for the Atlantic. This point is also illustrated empirically by a sharp reduction in natural radiocarbon concentrations poleward of the ACC, explained by the upwelling of old deep waters and very little poleward mixing of young surface to intermediate-depth waters across the current (e.g. see Fig. 6 of Kuhlbrodt et al. 2007). The relative isolation of the Southern Ocean is also demonstrated by its low rate of warming in response to anthropogenic greenhouse gas emissions, caused by upwelling of old unmodified waters and equatorward flow of surface waters (Armour et al., 2016).

The final aspect of interhemispheric coupling that we address here concerns the propagation of temperature anomalies to the Antarctic continent itself. In Stocker and Johnsen (2003) Antarctic temperatures simply follow the temperature of the proposed heat reservoir. The physics behind the actual coupling is beyond the scope of their thermodynamic model. Multiple coupled processes may be involved, including ocean and/or atmosphere forcing of sea-ice anomalies, sea-ice albedo feedbacks, anomalous atmospheric moisture and heat transport, heat release from Southern Ocean convection and anomalies in the top-of-atmosphere energy flux (see e.g. Otto-Bliesner and Brady, 2010; Timmermann et al. 2010; Menviel et al., 2015; Galbraith et al. 2016; Pedro et al. 2016a; b; Cabré et al. 2017). Literature on the factors controlling Antarctic temperature in the modern climate points to the importance of atmospheric circulation anomalies: two examples include the Southern Annular Mode's influence on Antarctic temperature via its affect on poleward atmospheric heat transport and Antarctic inversion layer strength (Gupta and England, 2007; Previdi et al., 2013); and the role of tropical Pacific SSTs in exciting atmospheric Rossby waves that affect atmospheric circulation over the Amundsen sea and associated atmospheric heat transport toward West Antarctica (Ding et al. 2011). AMOC perturbation experiments in intermediate complexity models have also pointed to the influence of atmospheric teleconnections, including from the tropical Atlantic (Buiron et al., 2012; Vettoretti and Peltier, 2015) and tropical Pacific (Timmermann et al. 2010), on regional variability in Antarctic temperatures. However there has not been any decomposition of the energy budgets in such experiments, as would be required to identify the relative roles of ocean, atmosphere and radiative processes.

2. Methods: transient GCM simulations

We use transient simulations conducted with the Community Climate System Model version 3 (CCSM3) to evaluate the thermal seesaw hypothesis. CCSM3 is a coupled atmosphere–ocean–sea-ice model with dynamic vegetation, 26 vertical atmospheric levels with T31 horizontal resolution and 25 ocean levels with nominal 3 degrees of horizontal resolution (Collins et al. 2006). The ocean model uses the Gent and McWilliams (1990) parameterisation of mesoscale eddy activity. The simulations were conducted as sensitivity runs during the Simulation of Transient Climate Evolution (TraCE) experiment (Liu et al. 2009; He, 2011; He et al. 2013). We refer to the simulations as the 'AMOC collapse' experiment, in which Greenland abruptly cools and Antarctica gradually warms, and the 'AMOC resumption' experiment, in which Greenland abruptly warms and Antarctica gradually cools. Note that in He (2011) these experiments are called DGL-19ka and DGL-Overshoot-C, respectively. In both experiments, freshwater perturbations are applied to the North Atlantic (80°W–20°E, 50°N–70°N) to alter the AMOC strength. Salt compensation was not applied in these simulations and there was no opening of any ocean straits or marginal seas in the model within the intervals studied.

As noted earlier, the bipolar seesaw hypothesis concerns the climate response to AMOC variations and not the cause of the AMOC variation itself (Stocker and Johnsen, 2003). In this context, and since our analysis is focused on the southern high latitudes where no freshwater is applied, we assume that our evaluation of the seesaw mechanism is relevant to the general case of AMOC variations, not just those forced by freshwater.

2.1. AMOC collapse experiment

The AMOC collapse experiment (Fig. 3, left panel) is used to examine the response of the southern high latitudes to a reduction in AMOC strength (where AMOC strength is defined here as the maximum meridional stream-function in the North Atlantic below 500 m). Throughout the experiment, ice sheet topography, greenhouse gases and orbital forcing are held constant at their 19 ka BP values. The AMOC is reduced by applying a constant 0.38 Sv freshwater flux to the North Atlantic for 300 years. Note that this freshwater forcing is larger than that applied in the simulation of Heinrich Event 1 in the TraCE-21k experiment (He, 2011, 0.17 Sv). On application of the freshwater, the AMOC is reduced ('collapses') by 10 Sv (from 13 to 3 Sv) within 150 years (Fig. 3a). When the freshwater flux is stopped, the AMOC begins to slowly recover, reaching 7 Sv by the end of the experiment. We consider 1000 years of model output, during which the first 500 years is from the TraCE simulation between 19.5 and 19.0 ka BP and the second 500 years is the experiment, in which the freshwater is immediately applied.

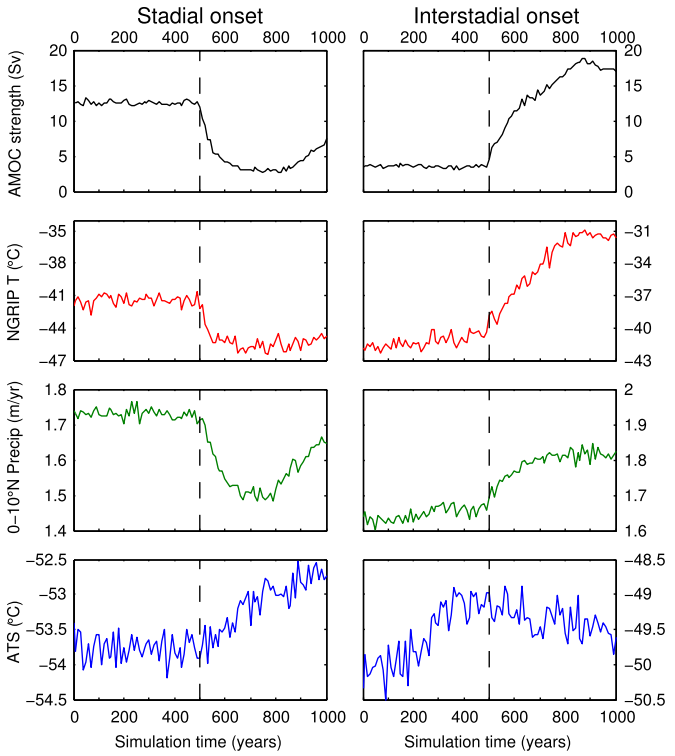

Fig. 3. Key modelled climate variables in the AMOC collapse experiment (left panel) and AMOC resumption experiment (right panel). From top: AMOC strength; surface temperature in the grid-cell corresponding to the NGRIP ice-core site; precipitation in the 0–10° North latitude band and the mean temperature in the grid cells corresponding to the Antarctic ice core temperature stack (ATS) that is displayed in Fig. 1. All data are annual means. Note that the temperature and precipitation vertical axes are offset between the two experiments. The dashed vertical lines mark the onset of the AMOC freshwater perturbations.

2.2. AMOC resumption experiment

The AMOC resumption experiment (Fig. 3, right panel) is used to examine the response of the southern high latitudes to an increase in AMOC strength. For this experiment, ice, greenhouse and orbital forcings are held constant at 14.90 ka BP values. During the first 500 years a constant 0.15 Sv freshwater flux is applied to the North Atlantic. The freshwater flux is then switched off and the AMOC increases from 3.5 Sv to 13 Sv within 150 years.

Ideally the collapse and resumption experiments would be conducted under the same boundary conditions, but since we make use of existing simulations this was not possible. Despite the

different boundary conditions we find that the pattern of anomalies and anomaly propogation are largely symmetric for the two experiments (i.e. of opposite sign).

2.3. Model evaluation

The kinematic proxy for AMOC circulation strength, $^{231}Pa/^{230}Th$, indicates near-complete AMOC collapse during Heinrich stadials, weakening during non-Heinrich stadials and reinvigoration to near-modern levels during interstadials (Henry et al., 2016). In the absence of more quantitative information on the amplitude of past AMOC variations, the ca. 10 Sv increase and decrease in AMOC strength in our experiments are reasonable scenarios for examining the thermal seesaw hypothesis. The strength of the Antarctic bottom water cell (i.e. the deep counter-clockwise circulating cell of the global ocean) is unchanged during our experiments at 20 Sv globally and 6 Sv for the component entering the Atlantic across 32°S. Since the thermal seesaw mechanism concerns the climate response to variations in the AMOC, the stability of the AABW cell is advantageous; i.e. it means that our analysis is not confounded by climate responses to changes in Antarctic bottom water formation.

In the AMOC collapse experiment, the modelled mean annual NGRIP air temperature drops by 5 °C in phase with the AMOC reduction (Fig. 3b). Most of this cooling is complete within the first 50 years. The amplitude and rate of change of the modelled NGRIP cooling is at the lower end of the range of the decadal-to-century-scale 5–10 °C coolings interpreted from NGRIP ice-core water stable isotope and nitrogen isotope data at Greenland stadial onsets (e.g. Kindler et al., 2014). The simulated cooling is strongest in winter (see Buizert et al., 2018, for detailed analysis of the seasonality of abrupt Greenland temperature change). The model mean precipitation in the northern tropics (0–10°) also abruptly drops in phase with AMOC collapse, signifying a southward migration of the Inter Tropical Convergence Zone (ITCZ). Abrupt southward shifts of the ITCZ at the onset of Greenland stadials are well-supported by tropical precipitation proxies from the Asian (e.g. Wang et al. 2001), African (e.g. Tierney et al., 2008) and central American (e.g. Peterson et al. 2000; Mosblech et al. 2012) monsoon regions. The southward shift of the ITCZ in response to cooling at northern high latitudes is also familiar from previous coupled model experiments (Vellinga and Wood, 2002; Chiang and Bitz, 2005; Zhang and Delworth, 2005; Kageyama et al., 2013) and explained dynamically by the progression of a cold SST front towards the ITCZ latitudes by atmospheric wind–evaporation–sea-surface-temperature feedbacks (see Chiang et al. 2008). In Antarctica, we see an initial ca. 100 yr period of little-to-no temperature change, before gradual warming at a rate of around 0.3 °C per century. The rate of warming is within the typical 0.1–0.3 °C per century inferred from ice-core water stable isotope trends during AIM warming stages (Fig. 1b, and see EPICA Community Members, 2006). Uncertainties in water stable isotope temperature reconstructions are discussed in detail in Jouzel et al. (1997).

In the AMOC resumption experiment, the NGRIP air temperature increases by around 10 °C following the AMOC increase, which is also in the range of the 5–16 °C temperature changes seen during Greenland interstadial transitions (see Fig. 1a and Buizert et al. 2014). The rate of NGRIP temperature change in the model appears slower than in the data, where the transitions (at least in water stable isotope composition) take place on a timescale of several decades to a century (Steffensen et al., 2008). The model mean precipitation increases in the 0–10°N latitude band, signifying that the ITCZ shifts to the north. As above, this pattern is robustly supported by proxy data and familiar from previous coupled model experiments. In Antarctica, a gradual cooling trend of around 0.1 °C per century accompanies the AMOC increase, also within the range of observations (Fig. 1b).

Overall, the simulated time series show amplitudes and rates of change that are consistent with palaeoclimate data. Most importantly, the trends in Antarctica—in the opposite hemisphere to where the freshwater was applied to trigger the AMOC variation—show rates of warming and cooling in agreement with the observed AIM events. A detailed comparison of the modelled Southern Hemisphere climate trends during the AMOC resumption experiment against marine, ice-core and terrestrial palaeoclimate proxies can be found in Pedro et al. (2016b). Throughout the analysis we focus primarily on the AMOC collapse experiment. The patterns of response in the AMOC resumption experiment are opposite and will be only briefly described.

3. Results

3.1. Compensating meridional ocean and atmosphere heat transports

To examine the Wunsch (2006) critique of the thermal seesaw model (Section 1.2) we consider how the meridional ocean and atmospheric heat fluxes adjust during the AMOC perturbations. The top panels of Fig. 4 show the climatological mean heat fluxes for the 100 years immediately prior to the AMOC perturbations (positive values signify northward heat transport, and negative values southward heat transport). The lower panels shows the mean heat flux anomalies for the time slice 200–300 years after the start of the respective AMOC perturbations (hereafter we denote such time slices in the form $t_{200-300}$).

In the AMOC collapse experiment the cross-equatorial Eulerian heat flux in the Atlantic drops from 0.65 PW to close to zero. The reduced Atlantic heat flux is largely compensated by increased northward heat flux in the atmosphere (+0.5 PW at the equator), consistent with the principle of Bjerknes compensation (Bjerknes, 1964). Previous coupled GCM experiments investigating AMOC perturbations show similar atmospheric compensation for changes in northward ocean heat flux; the increase in cross equatorial heat transport results from strengthening and southward migration of the NH winter Hadley Cell (Zhang and Delworth, 2005; Broccoli et al., 2006; Cheng et al., 2007), which allow the cell to transport more heat from the warm hemisphere to the cool hemisphere (Frierson et al., 2013; Hartmann, 2016). The meridional heat transport in the Indian and Pacific oceans also adjusts in response to the AMOC perturbations. In the AMOC collapse case, the northward Eulerian heat flux in the combined Indian and Pacific Oceans increases by +0.3 PW at the equator. The situation is reversed in the AMOC resumption experiment; northward heat transport in the Atlantic increases with the AMOC strengthening, while northward heat transport in the atmosphere and in the Pacific both decrease. However, the sum of the ocean and atmosphere heat transport anomalies (dashed lines in Fig. 4b and d) shows that the compensation is not perfect: in the case of AMOC collapse, total heat transport between ~ 20°S and Antarctica increases, whilst total heat transport between ~ 20°N and the Arctic increases. These heat transport anomalies are central to explaining the global pattern of climate response to AMOC perturbation, as discussed in Section 5.

3.2. Spatial pattern of temperature anomalies

The mean annual global surface temperature anomalies at $t_{200-300}$ are mapped in Fig. 5, the left panel shows the AMOC collapse experiment and the right panel shows the AMOC resumption experiment. Temperature anomalies in a meridional depth transect through the Atlantic Ocean for the same time slice are shown in the bottom panel. The temperature anomalies present

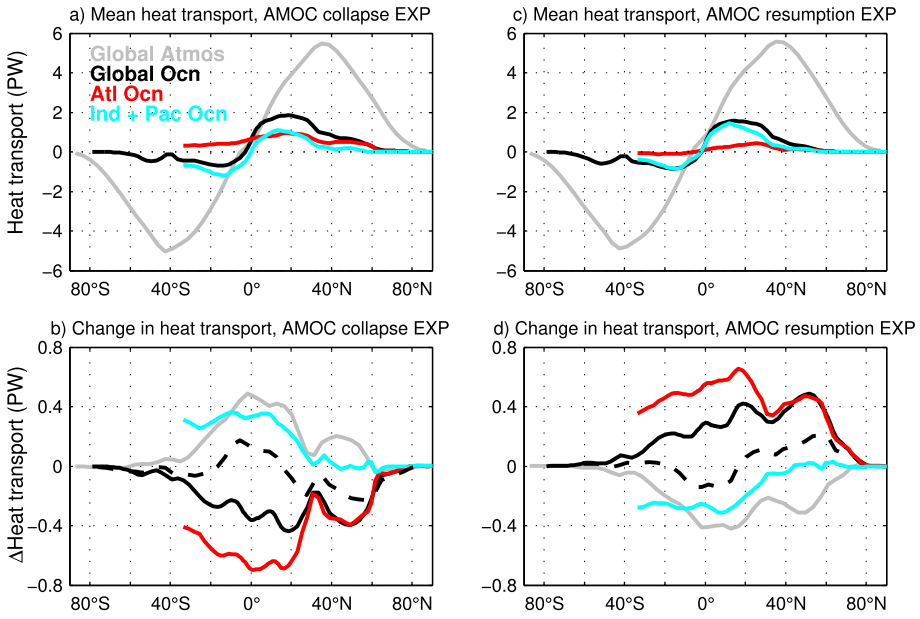

Fig. 4. Modelled meridional ocean and atmospheric heat transport climatologies and anomalies for the AMOC collapse and AMOC resumption experiments (annual mean data); including the global atmosphere, the global ocean, the Atlantic Ocean and the combined Pacific and Indian Ocean. The top panels show the mean heat transports for the 100 years prior to the AMOC perturbations. The lower panels show the mean heat transport anomalies for the period 200–300 years after the onset of the respective AMOC perturbations. The dashed line in the anomaly plots is the sum of the total atmosphere and total ocean anomaly. Positive values signify northward heat transport.

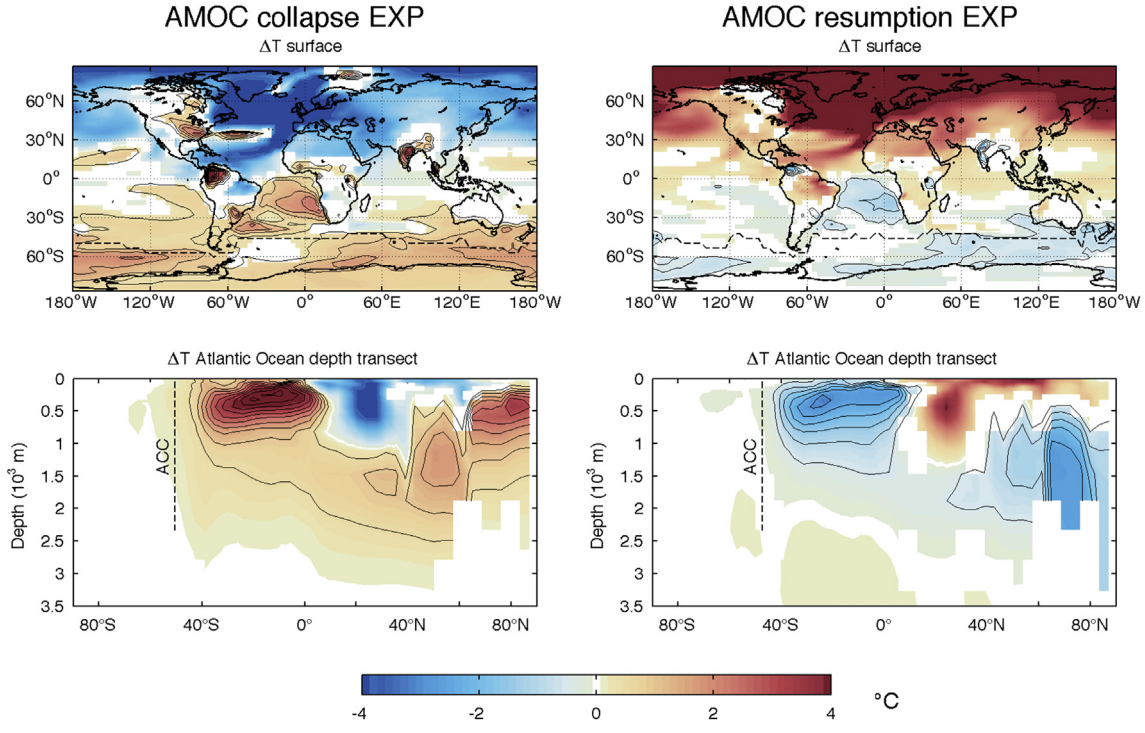

Fig. 5. Surface temperature anomalies (top) and Atlantic depth transect temperature anomalies (bottom) for the time slice 200–300 years after the onset of the respective AMOC perturbations. Anomalies are calculated with respect to the 100 years immediately prior to the AMOC perturbation. For the Atlantic Ocean depth transect we take the zonal mean between 30°W and 15°E. The dashed lines mark the position of the Antarctic Circumpolar Current (ACC) in the model (which we define by the surface maximum in zonal velocity). All shaded temperature anomalies are significant at the 95% confidence level (judged here and in subsequent figures using a two-sided Student's t-test). The contour spacing is 0.5 °C for all plots, the zero contour is omitted.

several challenges to the thermal bipolar seesaw hypothesis. We touch on these briefly below and return to them in more detail in the following sections.

The first challenge concerns the location and timing of the Atlantic temperature anomalies. The thermal seesaw hypothesis predicts that an AMOC collapse causes North Atlantic cooling and South Atlantic warming (and vice-versa for AMOC resumption). In the GCM, the North Atlantic cooling is restricted to the near surface

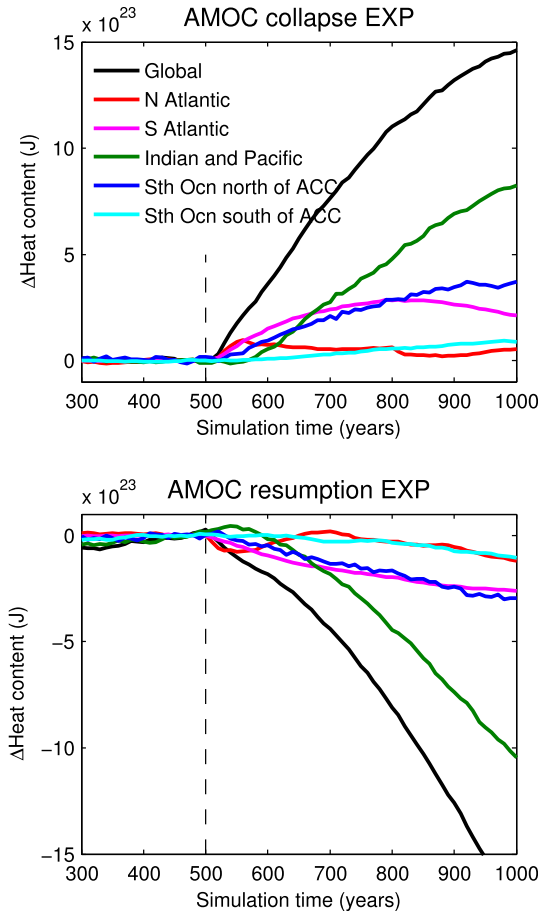

Fig. 6. Modelled changes in heat content of the global ocean and of specific ocean regions during the AMOC collapse (top) and AMOC resumption (bottom) experiments. Dashed vertical lines mark the start of the AMOC perturbations. We take 40°S as the northern boundary of the Southern Ocean.

layers and a deeper (1000 m) band between ca. 20 and 40°N. The latter cooling band follows the subduction path of the subtropical gyre, and is a typical result in experiments that change AMOC or gyre strength (Zhang and Liu, 1999; Jochum et al., 2008). Elsewhere in the North Atlantic the subsurface to intermediate depths warm (Fig. 5b). Overall the net heat content of the North Atlantic actually increases during the AMOC collapse (for the processes involved see Section 3.3). Similar subsurface North Atlantic temperature anomalies are seen in other recent GCM experiments, including those where the AMOC collapse results from freshwater discharge (Stocker et al., 2007; Galbraith et al., 2016) and from unforced internal oscillations (Peltier and Vettoretti, 2014).

In the South Atlantic, the AMOC collapse is associated with a warm anomaly that peaks at 4 °C around the depth of the subtropical thermocline (ca. 100–300 m). Temperature reconstructions from the southeast South Atlantic support a subsurface warming in this range for periods of major AMOC weakening during MIS 3 (Barker et al., 2009; Barker and Diz, 2014; Henry et al., 2016). Note that the modelled South Atlantic warm anomaly is not advected from the North Atlantic, rather it develops in situ (see Fig. 7, middle panel and Section 3.4).

The next challenge concerns the dynamic barrier presented by the Antarctic Circumpolar Current (ACC) to signal propagation between the South Atlantic and Southern Ocean (Section 1.2). The Atlantic Ocean temperature–depth transects show a steep meridional temperature gradient at the latitude of the ACC (Fig. 5, lower panel). In Section 3.3 we demonstrate that the Southern Ocean heat content south of the ACC has very little sensitivity to the AMOC perturbations. However, the radiative *surface* temperature anomalies in the sea ice zone (Fig. 5, upper panel) are as strong as those in the South Atlantic. This strong surface and weak subsurface temperature response south of the ACC is explained by changing sea ice concentrations; i.e. a fractional decease sea ice concentration means a fractional increase in (relatively warmer) ocean surface. The role of sea-ice feedbacks in the development of the climate signal and its propagation to the Antarctic continent is discussed in Section 3.5.

3.3. Ocean heat content

Fig. 6 shows how ocean heat content responds to the AMOC perturbations. In the AMOC collapse experiment, the heat content of the global ocean increases at a rate of $2–3\times10^{21}$ J/yr. This closely matches the rate of ocean heat content increase during Heinrich Stadial 1, of 2.6×10^{21} J/yr, recently inferred from Antarctic ice core noble gas mixing ratios (Bereiter et al., 2018). For context, the rate of increase in ocean heat content in recent decades due to anthropogenic global warming is 1×10^{22} J/yr (Levitus et al., 2012); i.e. three to five times faster than in our simulated AMOC collapse. Hence, although the simulated heat content change appears very large, it is much smaller than that resulting from the current anthropogenic greenhouse gas increase.

In the AMOC collapse experiment the North and South Atlantic account for essentially all of the global ocean heat content increase in the first 50 years. The increasing heat content of the North Atlantic reflects the dominance of the subsurface warming over the comparatively shallow layer of surface cooling (Fig. 5). The Southern Ocean heat content (where we define the Southern Ocean as the Ocean south of 40°S) behaves very differently on the northern and southern sides of the ACC: to the north of the ACC, the heat content begins increasing within around 50 years of the start of the AMOC perturbation; to the south of the ACC there is very little change in heat content throughout the entire experiment. The heat content of the Indian and Pacific Oceans begin to increase after around 100 years and after 300 years close to two thirds of the total increase in global ocean heat content is found in the combined Indian and Pacific basins. When weighted by basin volume, the response of the Southern Ocean is even more muted; it is the region of the global ocean with the slowest rate of change of heat content per unit volume.

In the case of AMOC resumption, these patterns are very similar but of opposite sign. Again, there is very little change south of the ACC. Overall the AMOC resumption is associated with a decrease in global ocean heat content, also at a rate of $2–3 \times 10^{23}$ J per century.

The change in global ocean heat content is due to the influence of the AMOC on the ocean–atmosphere heat flux (Galbraith et al., 2016). When the AMOC collapses, sea-ice expansion and a shutdown of convection means that heat loss from the high-latitude North Atlantic and Nordic seas to the atmosphere is greatly reduced (by 0.15 PW in the model), driving subsurface warming. The production and deep sinking of cold North Atlantic Deep Water is also reduced and the resulting warm anomaly is advected south in the Deep Western Boundary Current. In addition, the heat content of the South Atlantic increases due to thermocline deepening and reduced northward advection of heat in the AMOC upper limb.

The global ocean heat content increases, primarily in the top ca. 1500 m, as the Atlantic warm anomaly is propagated by advection and internal waves into the Indian and Pacific Ocean (see Section 3.4 for our more detailed treatment of the ocean signal propagation). When the AMOC strengthens, sea ice in the North Atlantic and Nordic Seas melts back, convection resumes and much more

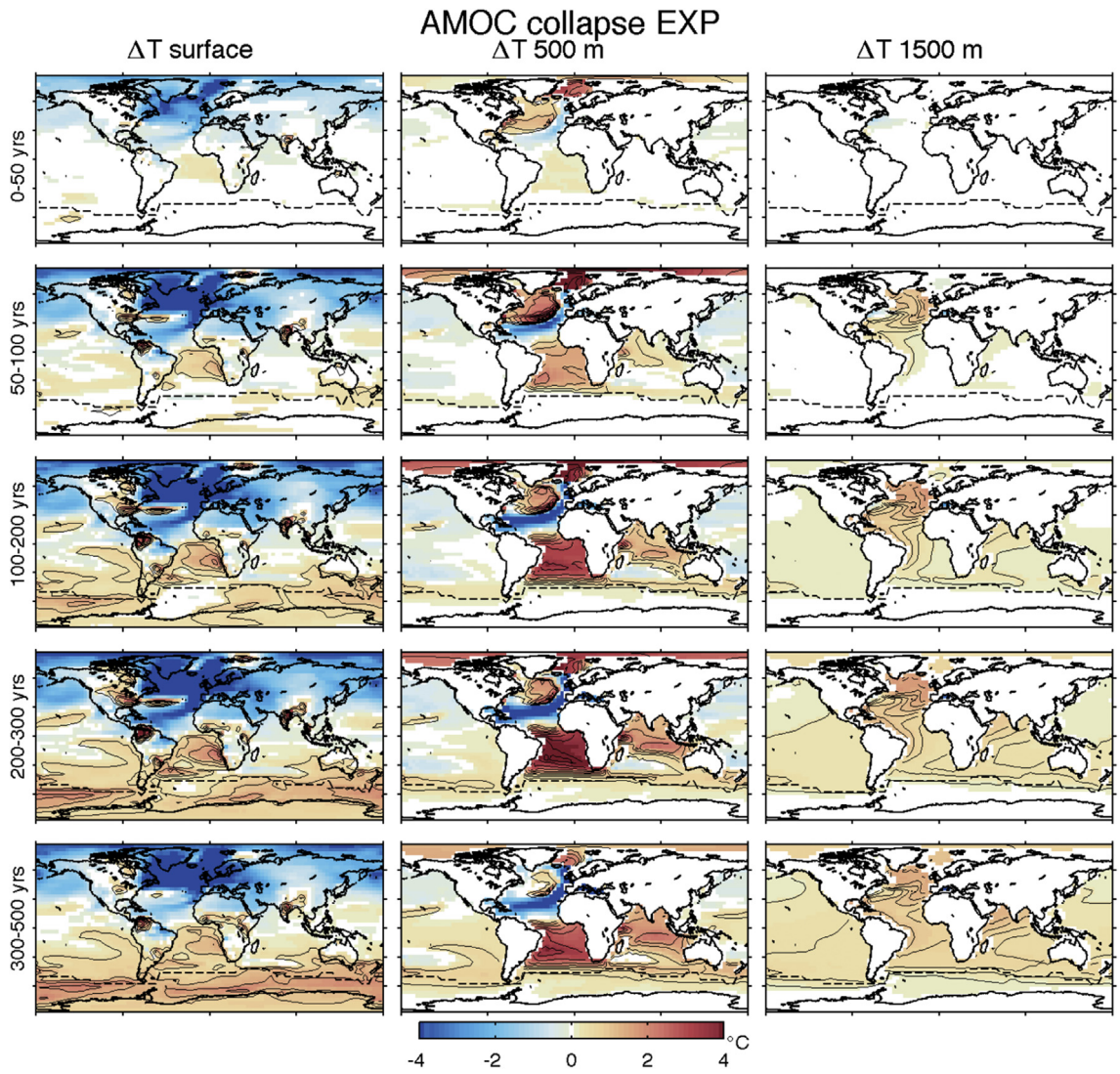

Fig. 7. Time evolution of temperature anomalies following AMOC collapse. Left panels show surface temperatures, middle panels 500 m ocean temperatures and right panels 1500 m ocean temperatures. The time slices (in years after the onset of the AMOC collapse) are marked on the left. Anomalies are calculated with respect to the 100 years immediately prior to AMOC collapse and all shading is significant at the 95% confidence level. The contour spacing is 0.5 °C for the surface and 500 m temperature plots and 0.2 °C for the 1500 m temperature plots, the zero contour is not shown. The ACC position during each time slice is marked by the dashed line.

heat is transferred from the subsurface ocean to the northern polar atmosphere, hence the interior ocean cools (Galbraith et al., 2016). Marine core observations from sites in the Nordic Seas (Dokken et al., 2013; Ezat et al., 2014; Rasmussen et al., 2016), northwestern Atlantic (Marcott et al., 2011) support that the subsurface and intermediate depths warm during Greenland stadials (most strongly during stadials containing Heinrich events) and cool during Greenland interstadials. Evidence of strong subsurface and intermediate-depth warming across the tropical Atlantic basin is also found during Heinrich stadial 1 (Weldeab et al. 2016).

These results challenge the common assumption that the Southern Ocean is a major heat reservoir during AMOC variations. Indeed, the region of the global ocean with the *smallest* change in heat content in these experiments is the Southern Ocean south of the ACC. During AMOC collapse the northern polar atmosphere and surface ocean cool and the global ocean interior warms; during AMOC resumption the northern polar surface ocean and atmosphere warms and the global ocean interior cools. Hence the 'see-sawing' of heat in these simulations is between the global ocean and the combined surface ocean and atmosphere at northern high latitudes.

3.4. Ocean signal propagation

To explore in more detail the pathways and timescales of temperature anomaly propagation in the global ocean during the AMOC perturbations, we consider the time evolution of temperature anomalies at the surface and on 500 m and 1500 m global ocean levels through time slices at t_{0-50}, t_{50-100}, $t_{100-200}$, $t_{200-300}$ and $t_{300-500}$. Fig. 7 shows the anomaly propagation in the AMOC collapse experiment and Fig. 8 shows the same for the AMOC resumption experiment. Signals can be transmitted in the ocean via advection, wave propagation and diffusion. The temperature anomalies at the surface, 500 m and 1500 m levels show evidence of all three processes at play.

Advection is identified on the 1500 m level where reduced North Atlantic deep-water formation during AMOC collapse results in a warm anomaly being slowly advected south in the Deep Western Boundary Current (DWBC) and then swept east in the ACC (Fig. 7, right panel). The flow speed in the modelled DWBC is on the

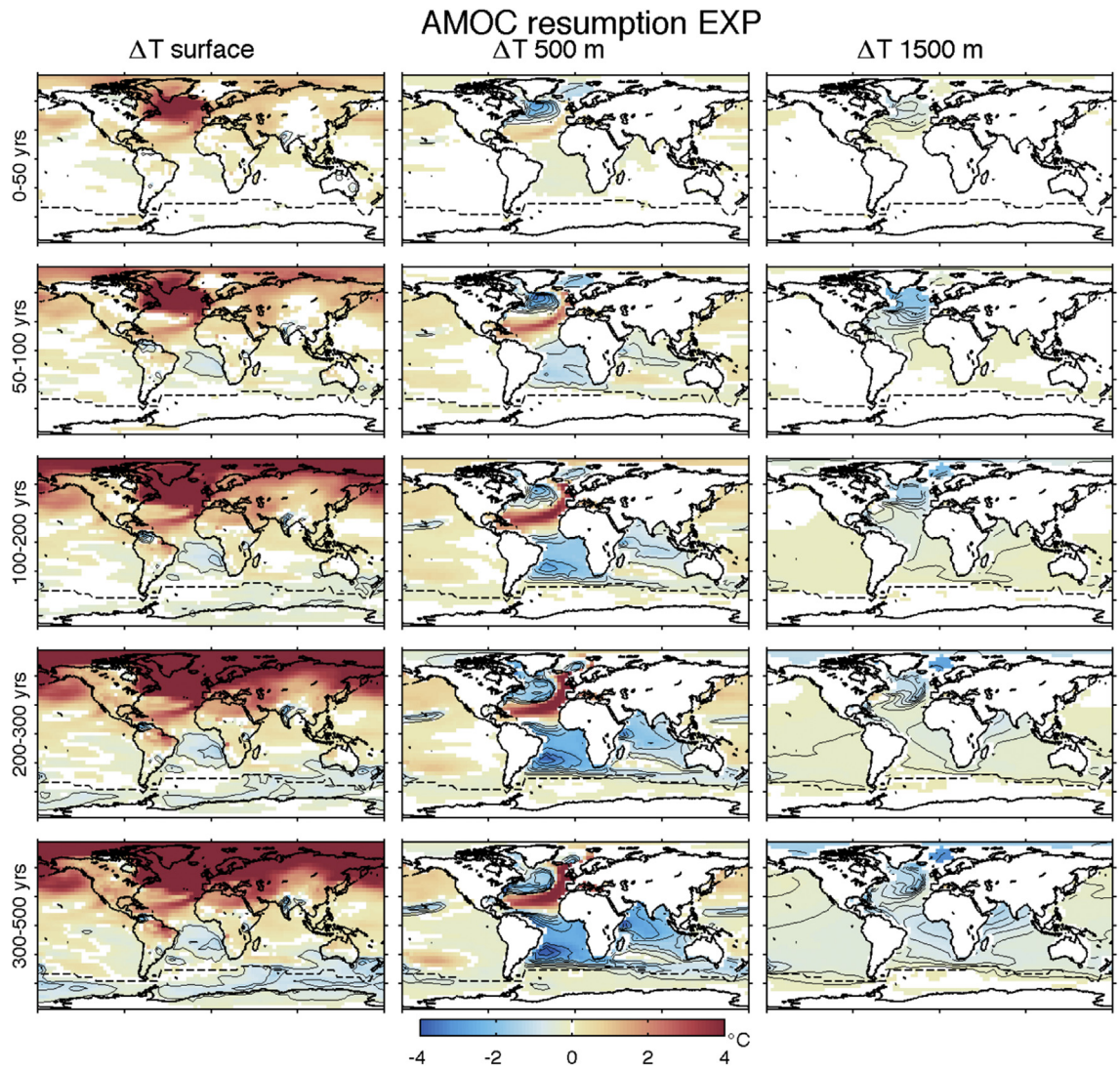

Fig. 8. Time evolution of temperature anomalies, as in Fig. 7, but for the AMOC resumption experiment.

order of cm/s, consistent with the signal taking around a century to cross the Atlantic. Signal propagation along the margins of the Indian and Pacific Oceans on the 1500 m level is explained by Kelvin and Rossby wave-driven deepening of the isopycnal in response to the change in North Atlantic Deep Water formation (Kawase, 1987; Huang et al., 2000). Because of the absence of a meridional boundary at the latitude of the Drake Passage, the signal cannot cross the ACC though Kelvin or Rossby waves. Nor can it be advected across the ACC, since by definition the flow is along the ACC axis. Thus, the signal has to cross the ACC with the help of eddy induced stirring and mixing (see also Section 3.5), these processes gradually mix a small temperature signal across the ACC, which is visible in Figs. 7 and 8 after around a century.

Marine cores show a strong temperature response in the subsurface tropical Atlantic and South Atlantic during AMOC collapse (Weldeab et al., 2016; Barker et al., 2009; Barker and Diz, 2014). Our results show this temperature change as well, most strongly across the subtropical thermocline and reaching down to around 1000 m (Fig. 5). Reduced northward advection of heat at all latitudes in the Atlantic is seen in our simulation following AMOC collapse (Fig. 4b). We also see an abrupt 50–100 m deepening of the tropical Atlantic and South Atlantic thermocline within a century of the AMOC collapse (see Fig. 9c and d). The reduced northward advection of heat and thermocline deepening together explain the subsurface maximum of the temperature anomaly and the associated storage of heat in the South Atlantic interior.

The abrupt thermocline deepening resembles, in amplitude and in speed, the Kelvin and Rossby-wave driven process described in Kawase (1987) and seen in the ocean-only model simulation of Huang et al. (2000). Reduced deep water production in the North Atlantic is equivalent to a source of upper-layer water and a sink of lower-layer water, causing a downward motion in the thermocline. Kelvin waves propogate the isopycnal deepening down the Atlantic western boundary toward the tropical Atlantic. The waves turn eastward at the equator and then upon reaching the African coast, propagate north and south along the Atlantic eastern boundary. Rossby waves spread the Kelvin wave-driven thermocline depth adjustments into the ocean interior.

Changes in winds over the South Atlantic (Fig. 9a and b) are also expected to affect the structure of the South Atlantic thermocline (see the adiabatic thermocline theory Luyten et al. 1983). Following AMOC collapse, the Atlantic ITCZ migrates south, which affects the wind field over the entire South Atlantic gyre. The wind changes also favour thermocline deepening and surface warming. First,

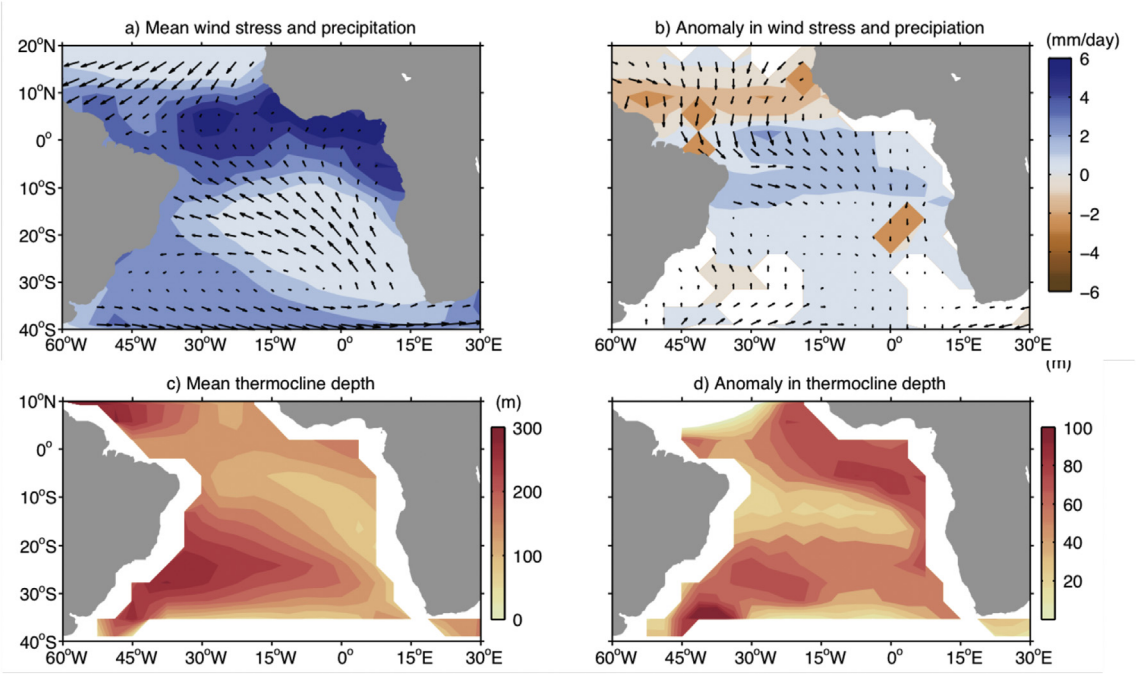

Fig. 9. Changes in South Atlantic wind stress, precipitation and thermocline depth in the AMOC collapse experiment for the time slice 50–100 years after the onset of AMOC collapse. a) Mean annual precipitation (shading) and wind stress (vectors). b) Anomaly in precipitation (shading) and anomaly in wind stress (vectors); note the southward shift of the ITCZ and southeasterly trades. c) Mean thermocline depth (defined here as the 11 °C isotherm). d) Anomaly in thermocline depth. Means are for the 100 years prior to the AMOC perturbation. The same colour bar applies to the precipitation mean and the precipitation anomaly maps. All plotted anomalies are significant at the 95% confidence level.

weakening of the southeasterly trades at the equator reduces evaporative cooling (Xie and Carton, 2004) and excites Kelvin waves that push down the thermocline as they propagate eastward across the basin and then southward down the African coast (as in modern day Atlantic warm events, e.g. Lübbecke, 2013). Second, weakening of the southeasterlies off the west coast of Africa reduces the cold Benguela upwelling (e.g. Nelson and Hutchings, 1983). Third, a 10–20% increase in wind-stress curl over the subtropical gyre, enhances the Ekman pumping of warm surface waters downward. Quantitative attribution of the South Atlantic thermocline deepening into advectively-driven, wave-driven and wind-driven components would require further simulations (see Section 6).

Wave propagation from the South Atlantic around the southern Africa carries the signal along the continental margins of the Indian Ocean within a few decades of AMOC collapse (Fig. 7 middle panel). The warm anomalies located on or just north of the ACC within the first 100 years result from southward adjustment of the ACC position in response to wind-stress changes (Section 3.5) and eastward advection of the South Atlantic warm anomaly with the ACC flow.

The temperature anomalies in the Atlantic sector of the Southern Ocean are smaller at the surface and on the 500 m level than anomalies in the Pacific and Indian sectors of the Southern Ocean. This non-zonality, which is also reflected in the sea ice anomalies, points again to the efficiency of wave propagation and advection in propagating the South Atlantic anomalies eastward.

3.5. Coupled changes in southern high-latitude atmosphere and ocean circulation

The AMOC collapse is followed by coupled changes in southern high-latitude atmospheric circulation, ocean circulation, sea ice concentration and surface temperature (Fig. 10 maps and Fig. 11 time series). Symmetric changes are seen in the case of AMOC resumption. The challenge is to establish the processes driving these coupled changes and their relationship to warming over the Antarctic continent itself.

We first consider the changes in atmospheric circulation. In the case of AMOC collapse, the poleward intensification of the westerlies, seen in the mean SH zonal wind (Fig. 10a) is a consequence of the large-scale adjustment of the Hadley circulation and associated southward shift of the ITCZ. The subtropical jet weakens on its northern margin and the eddy-driven jet (of which the surface expression is the mid-latitude westerlies) shifts southward. These adjustments are caused by reduced poleward transfer of angular momentum by the weakened SH Hadley cell. The angular momentum transfer argument explaining parallel shifts in the ITCZ and westerlies is discussed in detail elsewhere (Lee and Kim, 2003; Lee et al. 2011; Ceppi et al. 2013; Staten and Reichler, 2014). The southward shift of the westerlies is expressed as a positive anomaly in the Southern Annular Mode (SAM) index, which develops within 50–100 years of the onset of AMOC collapse (Fig. 10a, black line). Ice-core deuterium excess records from the WAIS Divide core indicate southward shifts of the WAIS moisture source region during Greenland stadial onsets (and vice-versa for interstadial onsets), consistent with the direction of the westerly shifts in the GCM (Markle et al. 2017).

The southward migration of the westerlies changes the surface wind stress (τ_x) felt by the Southern Ocean (Fig. 10b, map): the surface wind stress south of the ACC including over Drake Passage (Fig. 11, time series) is enhanced by ca. 10% and the surface wind stress north of the ACC is reduced. The surface wind stress controls the volume-transport of the ACC and the position of the associated sub-tropical, sub-Antarctic and polar fronts (Rintoul and Naveira Garabato, 2013). The southward shift in wind stress in the model thus explains the southward adjustment of the modelled barotropic stream function (Fig. 10c, map) and drives the 10 Sv (ca. 10%) increase in ACC flow through Drake Passage (Fig. 11, time series). The position of the maximum in zonal velocity, which we use to define the position of the ACC core, shifts south by a grid cell in a

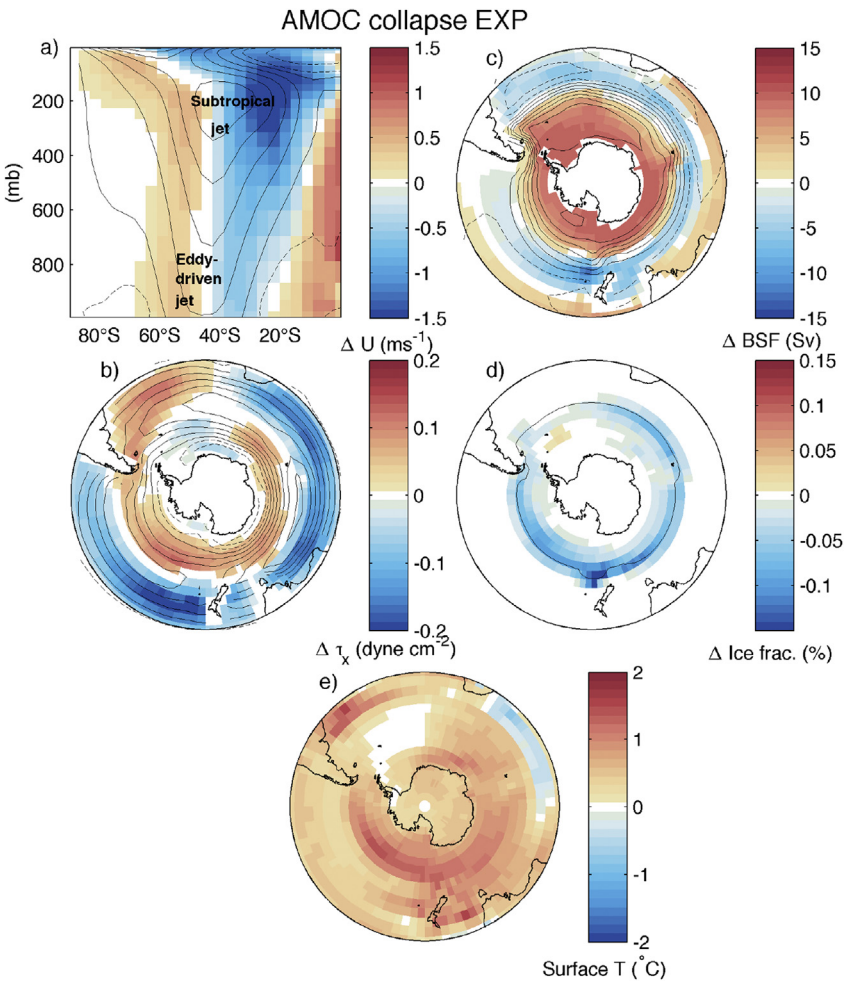

Fig. 10. Coupled changes in annual mean Southern Hemisphere atmospheric circulation, ocean circulation, sea ice extent and surface temperature in the AMOC collapse experiment. The anomalies for the time slice 0–300 years after the onset of AMOC collapse are shaded and the mean values for the 300-years prior to the AMOC perturbation are shown as contours (with solid contours denoting clockwise flow and dashed contours denoting anti-clockwise flow; zero contours are omitted): a) zonal mean zonal wind (U, contour spacing 7.5 ms^{-1}); b) surface wind stress (τ_x, contour spacing 0.4 dyne cm^{-2}); c) ocean barotropic stream function (BSF; contour spacing 30 Sv); d) sea ice fraction (the single contour marks the 15% ice fraction); e) surface temperature. All shaded anomalies are significant at the 95% confidence level.

few locations (see Fig. 7), but for the most part remains at the same latitudes, consistent with the topographic constraints on ACC flow (Rintoul and Naveira Garabato, 2013). Proxy evidence supporting an increased ACC flow speed through Drake Passage during Greenland stadials/AIM warmings is provided by grain size distribution in marine core sediments on the northern boundary of the Drake Passage (Lamy et al. 2015). A caveat to this result is that real-world ACC adjustments to wind-stress changes are sensitive to bathymetry, which is only coarsely resolved in the GCM, and to compensation by eddies, which are parametrized in the GCM; both are topics of ongoing debate in the physical oceanography literature (e.g. Rintoul and Naveira Garabato, 2013; Munday et al. 2013; Jochum and Eden, 2015; Bishop et al., 2016).

4. Energy budget of Antarctica and the Southern Ocean climate system during AMOC perturbation

Significant temperature anomalies south of the ACC correlate with the timing and spatial pattern of Southern Ocean sea ice retreat (Figs. 10 and 11d & e). We use an energy budget to diagnose the ocean, atmospheric, and radiative processes responsible for the sea ice retreat and for the resulting warming over the Antarctic continent itself.

We consider the anomalous energy budget of the Southern Ocean climate system (defined here as 50°S to 70°S) and of the Antarctic continent (defined here as 70° to 90°S). The energy budgets are composed of four primary terms: the net radiative flux at the top of the atmosphere (TOA), the air-sea heat flux (SHF), the total meridional atmospheric heat transport (MAHT, which is determined as a residual) and the total meridional ocean heat transport (MOHT). The MOHT is itself the sum of Eulerian mean advection ($MOHT_{Eulerian}$) and eddy-induced advection and diffusion ($MOHT_{eddy}$). Note that the MOHT terms are integrated over the entire ocean column.

To identify causality, we must also examine how the energy budget evolves with time during the AMOC perturbations. We consider three time slices: t_{0-100}, $t_{100-200}$ and $t_{200-300}$. The components of the energy budget are shown schematically in Fig. 12 for the $t_{200-300}$ time slice of the AMOC collapse experiment and its associated Antarctic warming. The components of the energy budget for each time slice are listed in Table 1 and 2 for the collapse and resumption experiments respectively.

The energy budget demonstrates that warming of the Southern Ocean climate system, which becomes significant 100-200 years after the onset of AMOC collapse, is primarily forced by an increase in southward ocean heat transport by eddies; the eddy heat flux across

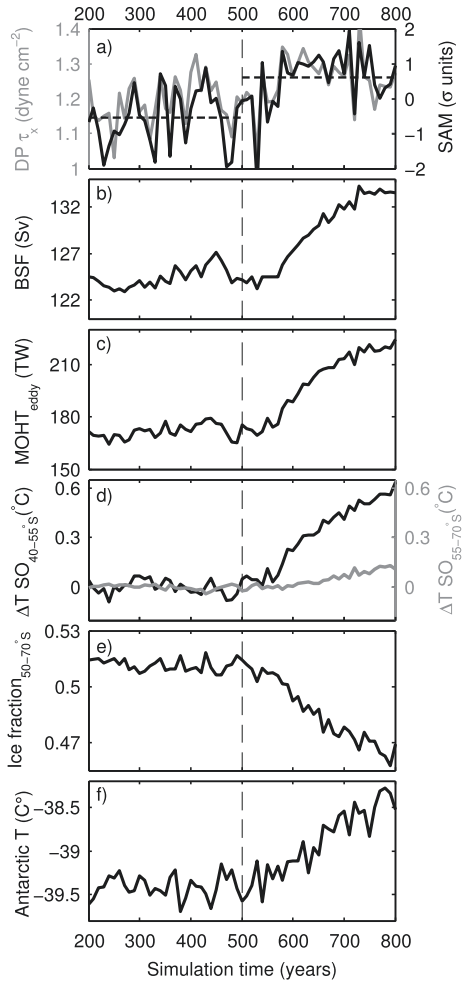

Fig. 11. Time series of southern high-latitude climate parameters during the AMOC collapse experiment (the onset of AMOC collapse is marked by the dashed vertical line). a) The Southern Annular Mode index (black) and surface wind stress (τ_x) in Drake Passage (grey). b) The barotropic stream function (BSF) through Drake Passage. c) Zonally and vertically integrated total *southward* meridional ocean heat transport by eddies ($MOHT_{eddy}$) across 50°S. d) Mean annual zonal ocean temperature anomaly between 40 and 55°S at 500 m depth (black) and mean annual zonal ocean temperature anomaly between 55 and 70°S at 500 m depth (grey). e) Mean annual 50–70°S sea ice fraction. d) Mean annual 70–90°S Antarctic surface temperature. The increase in the SAM index and in the Drake Passage wind stress are significant at the $p < 0.0001$ confidence level, according to a paired Student's *t*-test comparing the 300-year means before and after the onset of the AMOC perturbation; the dashed horizontal black lines in a) show the mean SAM index for these two time periods.

50°S increases by ca. 20% (corresponding to 37 TW, or 0.7 Wm^{-2} when averaged over the surface area of the 50°S to 70°S zonal band). The southward $MOHT_{eddy}$ flux itself has contributions from atmosphere and ocean forcing. The wind-forced southward shift of the barotropic stream function means that the Southern Ocean meridional temperature profile also shifts southward, bringing warmer waters into the sea ice zone. In addition, as the South Atlantic warm anomaly spreads eastward out of the South Atlantic and around the Indian and Pacific basins (on a timescale of around a century) the temperature gradient across the ACC increases (Fig. 7, map and Fig. 11d, time series). The increased temperature gradient, which is strongest in the thermocline and mostly confined to the upper 1500 m, means that eddy fluxes across the ACC transport more heat poleward as the AMOC perturbation progresses (Fig. 11c, time series).

Sea ice is sensitive to small changes in ocean temperature (Bitz and Polvani, 2012), and although the eddy heat transport across the ACC is small in terms of changes in Southern Ocean heat content, it is sufficient to initiate sea ice retreat and surface warming (Fig. 11d, time series). The surface warming is amplified by ice–albedo feedback: the top of the atmosphere energy input increases by 0.3 Wm^{-2} in the 50–70°S band, which is the sum of a 1.2 Wm^{-2} gain from incoming short-wave radiation (due to reduced albedo) and a 0.9 Wm loss from increased outgoing long-wave radiation (due to the surface and atmospheric warming).

As well as driving sea ice retreat, the increased eddy heat flux into the Southern Ocean contributes to an anomalous air-sea heat flux from the ocean to the atmosphere. The anomaly is relatively small (0.1 Wm^{-2}) averaged over the 50–70°S band, becoming larger further south (e.g. 0.4 Wm^{-2} when calculated over the 55–70°S band). This latitudinal difference occurs because of two opposing effects. First, more sensible and latent heat is released from the ocean in regions of sea ice loss. Second, more heat is taken up by the ocean around the polar front. The later increased uptake is because the southward intensification of the barotropic stream function causes a corresponding southward shift in the region of surface ocean heat and buoyancy gain.

As the surface and lower troposphere over the Southern Ocean warm, heat is mixed away meridionally; the poleward part of this anomalous atmospheric transport ($MAHT_{70°S}$) warms Antarctica. The poleward anomaly is negligible in the first 100 years, before increasing after 200–300 years to 0.6 Wm^{-2} when averaged over Antarctica. Latent and sensible heat release from close to the Antarctic coast also contribute to the Antarctic warming; small reductions in sea ice area within the 70–90°S band support an upward anomaly in the air-sea heat flux that reaches 0.4 Wm^{-2} after 200–300 years. Note that despite this anomaly, the Antarctic surface, in the mean, continues to take up heat from the atmosphere. The combined southward atmospheric heat transport and air-sea heat flux anomalies are sufficient to drive the ca. 0.1–0.2 °C per century Antarctic warming trend in the model, which is consistent with the rate of warming observed during AIM events (Fig. 1).

The energy budget for the AMOC resumption experiment (Table 2) shows that the same mechanisms apply (in the opposite direction) to drive Antarctic cooling: the eddy heat flux into the Southern Ocean climate system decreases; sea ice expands; ice–albedo feedback reduces energy input at the top of atmosphere and the associated reductions in air-sea heat flux cool the atmosphere. In turn, the atmospheric heat transport to Antarctica is reduced, cooling the continent.

In their transient simulation of Marine Isotope Stage 3 (MIS 3) using the LOVECLIM intermediate complexity model, Menviel et al. (2015) also found that increased heat fluxes across the ACC in response to AMOC collapse drove Southern Ocean SST anomalies. In their model, Southern Ocean and Antarctic surface temperatures warmed by up to 1 °C for the largest AIM events, falling short in rate of warming and in amplitude of the 2–3 °C anomalies seen in ice-core records. Additional experiments with an eddy-resolving ocean–sea-ice model (GFDL-MOM025) by these authors found greater spatial variability in temperature anomalies south of the ACC but not greater amplitude, possibly due to the absence of coupled air–sea feedbacks. In addition to AMOC perturbations, Menviel et al. (2015) also applied salinity anomalies to the Southern Ocean to drive changes in the lower cell of the meridional overturning (i.e. through changes in air–sea fluxes related to Antarctic Bottom Water formation). In contrast, the Antarctic warming in our experiment occurs without any changes in the lower cell, which remains stable through our experiments.

5. Discussion and conclusions

A stated objective of Stocker and Johnsen (2003) was to motivate future studies with more advanced models and high-

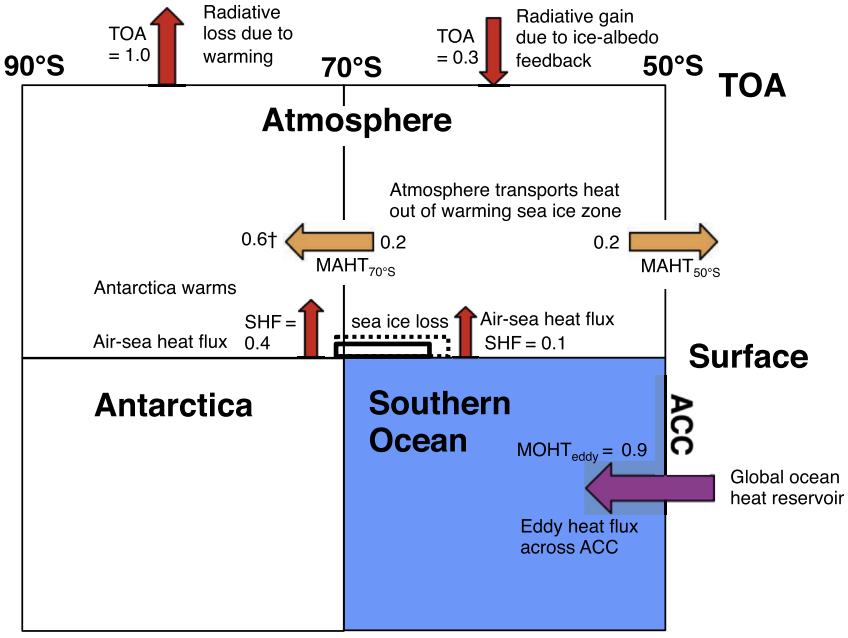

Fig. 12. Schematic of the ocean, atmosphere and radiative energy flux anomalies driving the simulated AIM warming of the AMOC collapse experiment. The arrows and fluxes correspond to the annual zonal mean energy budget anomalies for the Southern Ocean climate system (50–70°S) and Antarctic continent (70–90°S) during the $t_{200-300}$ time slice of the AMOC collapse experiment. The direction of anomalous heat transport is indicated by the arrows, all units are in Wm^{-2} averaged over the respective surface areas of these latitude bands, see Table 1 for values in TW and for other time slices. The fluxes involved in simulated AIM cooling are similar but of opposite sign (see Table 2). Abbreviations: Air-sea heat flux (SHF), total meridional ocean heat transport (MOHT); total meridional atmospheric heat transport (MAHT). †The poleward MAHT across 70°S is 0.2 Wm^{-2} *out of* the 50–70°S band and 0.6 Wm^{-2} *into* the 70–90°S, due to different surface areas of these bands.

Table 1
Zonal mean energy budget anomalies for the Southern Ocean climate system and Antarctic continent during the AMOC collapse experiment. The anomalies are expressed in Wm^{-2} averaged over the respective latitude bands (with anomalies in TW given in parentheses). The sign convention is defined so that positive anomalies contribute to warming of the atmospheric column in their respective latitude band. The mean annual energy budget terms are given for the t_{0-100}, $t_{200-300}$ and $t_{200-300}$ time slices (intervals in years after the start of the AMOC perturbation). Abbreviations: TOA, top of atmosphere; SHF, heat flux across the ocean–sea-ice–atmosphere interface; MAHT, total meridional atmospheric heat transport; MOHT, totoal meridional ocean heat transport.

Southern Ocean climate system (50–70°S)			
Flux	0–100 yrs	100–200 yrs	200–300 yrs
TOA	0.14 (7.2)	0.26 (14.5)	0.30 (16.7)
SHF	−0.02 (−1.0)	−0.1 (−5.3)	0.07 (4.1)
$MAHT_{50°S}$	0.03 (1.7)	−0.07 (−4.3)	−0.24 (−13)
$MAHT_{70°S}$	−0.02 (−1.2)	−0.10 (−5.6)	−0.17 (−9.2)
$MOHT_{total}$	0.03 (1.9)	0.36 (19.6)	0.73 (40.5)
$MOHT_{eddy}$	0.14 (7.4)	0.66 (36.6)	0.88 (48.7)
Antarctic continent (70–90°S)			
TOA	−0.16 (−2.3)	−0.58 (−8.4)	−0.99 (−14.4)
SHF	0.08 (1.2)	0.19 (2.8)	0.36 (5.2)
$MAHT_{70°S}$ [a]	0.08 (1.2)	0.38 (5.6)	0.63 (9.2)

[a] The different Wm^{-2} values for $MAHT_{70°S}$ for the 50–70°S and 70–90°S bands reflect their different surface areas.

Table 2
As for Table 1, but for the AMOC resumption experiment. Sign convention: positive anomalies contribute to warming of the atmospheric column in their respective latitude bands.

Southern Ocean climate system (50–70°S)			
Flux	0–100 yrs	100–200 yrs	200–300 yrs
TOA	−0.15 (−8.3)	−0.09 (−4.8)	−0.14 (−7.6)
SHF	−0.02 (−1.3)	−0.16 (−8.7)	−0.38 (−21.0)
$MAHT_{50°S}$	0.08 (4.6)	0.13 (7.4)	0.40 (21.9)
$MAHT_{70°S}$	0.00 (0.0)	0.07 (3.7)	0.06 (3.2)
$MOHT_{total}$	−0.031 (−1.7)	−0.28 (−15.3)	−0.33 (−18.4)
$MOHT_{eddy}$	−0.17 (−9.1)	−0.53 (−29.4)	−0.74 (−40.7)
Antarctic continent (70–90°S)			
TOA	−0.03 (−0.4)	0.27 (3.9)	0.35 (5.1)
SHF	−0.03 (−0.4)	−0.05 (−0.7)	−0.17 (−2.5)
$MAHT^{\dagger}_{70°S}$	0.00 (0.00)	−0.25 (−3.7)	−0.22 (−3.2)

resolution climate data to resolve the details of the physical and dynamical processes involved in interhemispheric coupling. In the context of using past climate variability to improve our understanding of the climate system, it is the detailed process understanding that is needed. Our intention with this review has been to take up the challenge of moving from a conceptual toward a process-based understanding of interhemispheric coupling and the forcing of AIM events. We have examined limitations of the thermal seesaw relating to meridional heat transport in the coupled climate system, signal propagation in the Atlantic, the heat reservoir location and means of operation and anomaly propagation to the Antarctic continent. We now discuss and summarise our findings in each of these areas.

Cross-equatorial heat transport in the Atlantic responds sensitively to AMOC perturbation in the GCM, as is assumed by the thermal seesaw. However, the changes in Atlantic heat transport are largely compensated by opposing changes in cross-equatorial heat transport in both the global atmosphere and the Pacific Ocean. These opposing changes in ocean and atmospheric heat transport are fundamental to explaining the spatial pattern of the climate anomalies (see also Cheng et al., 2007): in the case of AMOC collapse, abrupt cooling in the northern high latitudes means that the thermal equator, and with it the Hadley circulation and ITCZ, are displaced south, as evidenced by tropical precipitation proxies (e.g Peterson et al., 2000; Wang et al., 2001; Tierney et al., 2008; Mosblech et al., 2012; Cheng et al., 2013).

Energy transport in the upper limb of the Hadley circulation slightly exceeds that in the lower limb (due to the moist static energy profile in the tropics). The southward shift of the ITCZ, i.e. toward the warmer hemisphere, thus means that the cross-equatorial Hadley cell gathers more energy in its lower southward limb for transport across the equator in its upper limb into the northern hemisphere (Kang et al. 2008). Atmospheric energy transfer from the Hadley circulation to the higher latitudes occurs via atmospheric jets and eddies. Hence the change in meridional atmospheric heat transport also manifests in the adjustment of the subtropical jet and the mid-latitude westerlies (Lee et al. 2011; Ceppi et al. 2013). The role of these compensating meridional heat transports in the stability of the AMOC warrants further study. Poleward migration of the westerlies at the onset of Greenland stadials (and equatorward at the onset of interstadials) is supported by ice-core deuterium excess data from the WAIS Divide core (Markle et al. 2017). Further observational support for adjustment of the westerlies during the stadial/interstadial transitions (at least for the last deglaciation) is provided by Chilean-margin marine cores (Lamy et al. 2007), Patagonian lake records (Moreno et al. 2012) and New Zealand mountain glacier reconstructions (Putnam et al. 2010). Previous studies have suggested that southward-shifted and/or strengthened westerlies could increase the wind-driven upwelling of relatively warm (compared to the surface) deep water, contributing to AIM warming through release of heat and CO_2 from the Southern Ocean (Anderson et al., 2009; Lee et al., 2011). Although we cannot exclude this mechanism, we do not detect any increased upwelling in our simulation in response to the changed westerlies.

Turning now to signal propagation in the Atlantic Ocean. The original Atlantic seesaw concept of Crowley (1992) attributed opposing changes in North and South Atlantic temperature to a changes in the cross-equatorial advection of heat in the Atlantic. In the GCM, the AMOC collapse is accompanied by reduced northward advection of heat in the AMOC upper limb and a decadal-scale deepening of the South Atlantic thermocline. The thermocline deepening is consistent with the abrupt sub-surface warming seen in tropical and South Atlantic marine sediment core records during periods of reduced AMOC (Weldeab et al., 2016; Barker et al., 2009).

The reduced northward advection provides a source of heat to warm the South Atlantic while the thermocline deepening allows the heat to be stored at depth rather than released to the atmosphere through the Ekman layer (see e.g. Liu et al., 1994). The timescale and amplitude of the thermocline deepening is consistent with a basin-wide Kelvin and Rossby wave-propagated isopycnal deepening in response to reduced North Atlantic deep water formation (Kawase, 1987; Huang et al., 2000; Schmittner et al., 2003). The simulated wind-stress changes over the South Atlantic gyre also act in the direction of deepening the thermocline: following AMOC collapse, the well-documented southward shift of the ITCZ is associated with a weakening of the southeasterly trades at the equator and a weakening of the wind-stress over the Benguela upwelling region (in line with marine and terrestrial climate records Kim et al. 2003; Chase et al. 2015). These are the same wind changes that drive modern-day Atlantic warm events (Lübbecke, 2013) and in the simulation they are accompanied by increased wind-stress curl over the South Atlantic gyre, promoting Ekman pumping of warm surface waters downward.

We note that previous ocean-only model experiments show South Atlantic warming (in response to AMOC collapse) of similar amplitude to that in our coupled run (e.g. Schmittner et al., 2003), which may be considered an argument against the role of winds in the thermocline deepening. However, ocean-only models lack atmospheric feedbacks (including air-sea fluxes and changed Ekman transport), which could otherwise dampen or strengthen such temperature anomalies. In our coupled simulation, advection, wave propagation and wind forcing all appear to act in a way that is mutually reinforcing for warming and thickening the South Atlantic thermocline. The interplay between these processes (or lack of) may explain why some coupled models exhibit only a weak South Atlantic warming during AMOC collapse (e.g. Kageyama et al., 2013).

A key result of our review concerns the location and operation of the postulated heat reservoir. In Stocker and Johnsen (2003), heat diffuses out of the South Atlantic into a heat reservoir, commonly assumed to be the Southern Ocean. We tested this assumption by quantifying the change in heat content of the major ocean basins across the AMOC perturbations. We find that the global ocean heat content increases in the case of AMOC collapse and that the Southern Ocean comprises only a minor share of this increase. The increased global ocean heat content during AMOC collapse results from two main factors: first, the expansion of sea ice and shutdown of convection in the high-latitude North Atlantic and Nordic Seas reduces ocean heat loss to the atmosphere (Galbraith et al., 2016), driving a subsurface warm anomaly that propagates south in the Deep Western Boundary Current; second, reduced northward advection and thermocline deepening permit increased heat storage in the South Atlantic. The combined Indian and Pacific—not the Southern Ocean—dominate the increase in global ocean heat content, because temperature anomalies propagate eastward out of the South Atlantic and along continental boundaries into the Indian and Pacific (by Kelvin and Rossby waves) and eastward with the ACC flow (by advection) much more efficiently than they can propagate south across the ACC (which relies on eddy fluxes) (Cox, 1989; Schmittner et al., 2003).

Hence, we support the Stocker and Johnsen (2003) hypothesis that a thermal reservoir integrates North Atlantic temperature change during AMOC perturbations, but suggest that the reservoir location is the global ocean interior rather than the Southern Ocean. Another argument against a Southern Ocean heat reservoir is that the centennial-scale thermal inertia of the Southern Ocean (Knutti et al. 2004) does not fit with the 1000 to 1500 year thermal seesaw time constant proposed by Stocker and Johnsen (2003); the millennial timescale of global ocean thermal inertia affords a better

match.

Our final key result concerns signal transmission from the Southern Ocean to the Antarctic continent. In Stocker and Johnsen (2003) Antarctic temperature is assumed to vary in phase with the heat content of the proposed Southern Ocean heat reservoir. In the GCM we traced the thermal, dynamic and radiative processes driving Antarctic temperature change. Thermally, warming on the northern margin of the ACC, which extends from the Atlantic to the Pacific on a timescale of around a century, enhances the poleward temperature gradient in the top 1500 m (Figs. 5 and 7), causing an increase in the poleward eddy heat flux across the ACC. Dynamically, southward migration of the mid-latitude westerlies (resulting from the change in Hadley circulation), causes poleward intensification of the ACC and southward adjustment of the Southern Ocean temperature profile. Although the resulting temperature anomalies to the south of the ACC in our simulation are small (ca. 0.1 °C), the sensitivity of sea ice production and melt to small ocean temperature anomalies drives sea ice retreat (Bitz and Polvani, 2012), which is then amplified by the ice–albedo feedback. The energy input from increased poleward eddy heat flux and from the ice–albedo feedback warm the lower troposphere in the Southern Ocean sea ice zone. Antarctic warming then results from the atmosphere mixing heat and moisture out of the warming sea ice zone towards Antarctica (Fig. 12). The increase in poleward heat and moisture transport would both contribute to the more positive water stable isotope ratios seen during AIM events. When the AMOC resumes, the same processes operate in the opposite sense to drive Antarctic cooling.

Putting these results together, we summarise the chain of events driving the warming stage of an AIM event as follows. The weaker AMOC that is associated with the onset of Greenland stadials leads to a reduction in northward advection of heat at all latitudes in the Atlantic and a southward shift of the ITCZ. The ITCZ shift weakens the equatorial southeasterlies, deepening the equatorial and then, through planetary wave connections, the subtropical thermocline. The reduced northward advection and thermocline deepening allow heat to accumulate in the South Atlantic interior and spread eastward into the Indian and Pacific, which increases the circumpolar temperature gradient across the ACC on a timescale of around a century. Warmer water is then mixed by eddies across the ACC, in turn increasing the poleward ocean heat flux and driving sea ice retreat. This initial warming is amplified through ice–albedo feedback. The atmosphere overlying the Southern Ocean in turn warms, providing more heat for the atmospheric heat flux to Antarctica.

In our simulations the interior ocean and Antarctic warming trends both continue for as long as the AMOC remains shut down. The eddy heat flux across the ACC connects the Southern Ocean sea ice zone to the global ocean heat reservoir, thus providing the sustained energy source to drive centennial to millennial-scale Antarctic warming. In this context, we suggest that Antarctic temperature is a proxy for *global* ocean heat content during the DO and AIM variations. Evidence from noble gas mixing ratios in Antarctic ice cores, a proxy for mean ocean temperature (Headly and Severinghaus, 2007), lends support to our suggestion: Antarctic temperature and noble-gased based mean ocean temperature (and thus heat content) vary in parallel during the abrupt climate events of the last glacial termination (Bereiter et al., 2018). Quantitatively, the rate of change of global ocean heat content during Heinrich Stadial 1 reported in Bereiter et al. (2018) closely matches that in our simulation (both are in the range $2–3\times10^{21}$ J/yr). Notably, these authors report an even higher rate of increase, potentially exceeding the modern anthropogenic signal, as Antarctic warms at the start of the Younger Dryas.

The onset of Antarctic temperature change in our simulations lags the abrupt change in Greenland by around a century. By comparison, ice-core data suggests Antarctic warming lags Greenland transitions by 208±96 years. In the GCM the lag is dominated by the time taken for the warm anomaly to spread from the Atlantic around the northern margin of the ACC; once the southward eddy heat transport increases, sea ice retreat and atmospheric heat transport toward Antarctica follow without any obvious delay. The GCM results lend support to the WAIS Divide Project Members (2015) and Schmittner et al. (2003) suggestions that the presence of the ACC is what slows the propagation of the DO signal to Antarctica; our contribution with the GCM has been to document the processes by which the ACC is crossed and how the signal then reaches Antarctica. Additional experiments are needed to test whether the lag would change in an eddy-permitting ocean model and/or whether it is sensitive to different eddy parameterisation schemes (e.g. Eden et al. 2009). We also expect that the lag may be sensitive to the speed of the AMOC collapse and resumption, which are yet poorly constrained by observations. Note that the ca. 200-year lag of the onset of AIM warming behind the Greenland stadial transitions is only apparent when averaging over multiple AIM events at a given site (WAIS Divide Project Members, 2015) or over multiple sites for a given AIM event (Raisbeck et al. 2017). This is unsurprising if we are correct about the relatively small forcing (ca. 0.6 Wm^{-2}) driving the Antarctic warming signal, which is of the same scale as internal variability in poleward heat transport (Previdi et al., 2013): i.e. apparent differences in the timing of AIM onsets between events and between sites could easily reflect internal variability in poleward heat transport imprinted on top of the longer-term energy imbalance driving the AIM events.

6. Future work

We conclude by listing some caveats of our study and suggestions for future work.

(1) Targeted sensitivity experiments are needed to quantify and separate the relative contributions of a) changed advection, b) Kelvin and Rossby wave propagation from the North Atlantic and c) changed winds, to thermocline depth adjustment and heat storage in the South Atlantic gyre. In particular, we suggest comparing AMOC perturbation experiments in coupled and ocean-only configuration with experiments in which the changes in equatorial wind stress are applied *without* AMOC perturbation.

(2) Our energy budget analysis indicates that warming in the Southern Ocean sea ice zone during the AMOC collapse is driven primarily by increased eddy-heat flux across the ACC in response to warming on the ACC northern margin. Constraining the influence of wind-stress changes on the ACC position and intensity, and in turn the wind-stress contribution to warming in the Southern Ocean sea ice zone, requires targeted experiments with eddy-resolving models. Such research overlaps with (and can potentially provide insight into) current efforts to understand the role of wind changes on modern Southern Ocean circulation, heat uptake and sea ice conditions. The potential for sea ice anomalies to feed back on the position of the westerlies during DO and AIM events also requires further investigation (see e.g. Gupta and England, 2007, for evidence of such feedbacks operating in the modern climate system). It seems unlikely that sea ice retreat itself forces the poleward intensification of the eddy-driven jet in the GCM, since sea ice retreat should act in the direction of displacing the jet equatorward rather than poleward (Sime et al. 2016).

(3) As also mentioned by Stocker and Johnsen (2003), more research is needed on atmosphere–ocean interaction in areas of convection and sea ice formation in the Southern Ocean. Increased heat exchange across the ACC could trigger Southern Ocean deep convection, which would amplify both the mid- and high-latitude warming by enhancing heat release from Southern Ocean intermediate depths (e.g. Martin et al. 2015; Pedro et al. 2016a; Cabré et al. 2017). We do not exclude that deep convection around Antarctica (and Antarctic bottom water production) did change in response to real-world DO/AIM events, with contributions to the observed AIM signatures (e.g. Menviel et al., 2015).

(4) More work is also needed on the controls on water stable isotopes in coastal and inland Antarctica. The transport of sensible heat and moisture to Antarctica increase in our simulations as sea ice retreats. Our zonal mean treatment of the energy budget does not resolve internal differences in these transports between sectors. Non-zonalities in the energy fluxes are also expected and may explain regional differences in ice-core signals, such as the different structure of AIM signals at the EDML site in the Atlantic sector compared to sites on the East Antarctic Plateau (Landais et al., 2015). Performing a similar experiment with an isotope-enabled model and with a non-zonal decomposition of the energy budget could aid in resolving the cause of such regional differences.

(5) An important caveat of our study is the assumption that our results are relevant to the general case of AMOC variations, not just those forced by freshwater. This assumption is lent some support by the coupled model study of Brown and Galbraith (2016), which finds that the global climate response to AMOC perturbation is quite consistent between simulations with freshwater-forced and unforced AMOC perturbations. A systematic comparison of the Southern Hemisphere climate response in a range of models in which AMOC variations result from different processes is needed to fully test this assumption.

Acknowledgments

This research was supported by the European Research Council under the European Communitys Seventh Framework Programme (FP7/2007–2013)/ERC grant agreement 610055 (the *ice2ice* project). JBP acknowledges financial support from the European Union Horizon 2020 research and innovation programme under Marie Skłodowska Curie grant agreement 330552. CB acknowledges financial support from the US National Science Foundation (ANT 1643394). We thank participants in the *ice2ice* Southern Ocean and MIS 3 workshop and also Thomas Stocker, Laura Herraiz Borreguero, Helen Bostock, Torge Martin, Jonathan Rheinlænder and Eric Steig for stimulating discussions that helped inspire this paper. We are grateful for constructive feedback from two anonymous reviewers. We thank Roman Nuterman for coding assistance.

References

Adkins, J.F., Cheng, H., Boyle, E.A., Druffel, E.R.M., Lawrence Edwards, R., 1998. Deep-sea coral evidence for rapid change in ventilation of the deep North Atlantic 15,400 years ago. Science 280 (May), 725.

Anderson, R.F., Ali, S., Bradtmiller, L.I., Nielsen, S.H.H., Fleisher, M.Q., Anderson, B.E., Burckle, L.H., 2009. Wind-driven upwelling in the Southern Ocean and the deglacial rise in atmospheric CO_2. Science 323 (Mar.), 1443.

Armour, K.C., Marshall, J., Scott, J.R., Donohoe, A., Newsom, E.R., 2016. Southern Ocean warming delayed by circumpolar upwelling and equatorward transport. Nat. Geosci. 9 (July), 549–554.

Banderas, R., Alvarez-Solas, J., Robinson, A., Montoya, M., 2015. An interhemispheric mechanism for glacial abrupt climate change. Clim. Dyn. 44 (May), 2897–2908.

Barker, S., Diz, P., 2014. Timing of the descent into the last Ice Age determined by the bipolar seesaw. Paleoceanography 29 (June), 489–507.

Barker, S., Diz, P., Vautravers, M.J., Pike, J., Knorr, G., Hall, I.R., Broecker, W.S., 2009. Interhemispheric Atlantic seesaw response during the last deglaciation. Nature 457 (Feb.), 1097–1102.

Barker, S., Knorr, G., Vautravers, M.J., Diz, P., Skinner, L.C., 2010. Extreme deepening of the Atlantic overturning circulation during deglaciation. Nat. Geosci. 3 (Aug.), 567–571.

Bender, M., Sowers, T., Dickson, M.-L., Orchardo, J., Grootes, P., Mayewski, P.A., Meese, D.A., 1994. Climate correlations between Greenland and Antarctica during the past 100,000 years. Nature 372 (Dec.), 663–666.

Bereiter, B., Shackleton, S., Baggenstos, D., Kawamura, K., Severinghaus, J., 2018. Mean global ocean temperatures during the last glacial transition. Nature 553 (Jan.), 39–44.

Bishop, S.P., Gent, P.R., Bryan, F.O., Thompson, A.F., Long, M.C., Abernathey, R., 2016. Southern Ocean overturning compensation in an eddy-resolving climate simulation. J. Phys. Oceanogr. 46 (May), 1575–1592.

Bitz, C.M., Polvani, L.M., 2012. Antarctic climate response to stratospheric ozone depletion in a fine resolution ocean climate model. Geophys. Res. Lett. 39 (Oct.), L20705.

Bjerknes, J., 1964. Atlantic air/sea interaction. Adv. Geophys. 10, 1–82.

Blunier, T., Brook, E.J., 2001. Timing of millennial-scale climate change in Antarctica and Greenland during the last glacial period. Science 291 (Jan.), 109–112.

Blunier, T., Chappellaz, J., Schwander, J., Dällenbach, A., Stauffer, B., Stocker, T.F., Raynaud, D., Jouzel, J., Clausen, H.B., Hammer, C.U., Johnsen, S.J., 1998. Asynchrony of Antarctic and Greenland climate change during the last glacial period. Nature 394 (Aug.), 739–743.

Bond, G.C., Lotti, R., 1995. Iceberg discharges into the North Atlantic on millennial time scales during the last glaciation. Science 267 (Feb.), 1005–1010.

Broccoli, A.J., Dahl, K.A., Stouffer, R.J., 2006. Response of the ITCZ to northern hemisphere cooling. Geophys. Res. Lett. 33 (Jan.), L01702.

Broecker, W., 1998. Palaeocean circulation during the last deglaciation: a bipolar seesaw? Paleoceanography 13, 119–121.

Broecker, W.S., Denton, G.H., 1989. The role of ocean-atmosphere reorganizations is glacial cycles. Geochimica Cosmochimica Acta 53 (Oct.), 2465–2501.

Broecker, W.S., Peteet, D.M., Rind, D., 1985. Does the ocean-atmosphere system have more than one stable mode of operation? Nature 315 (May), 21–26.

Broecker, W.S., Bond, G., Klas, M., Bonani, G., Wolfli, W., 1990. A salt oscillator in the glacial Atlantic? 1. The concept. Paleoceanography 5 (Aug.), 469–477.

Brown, N., Galbraith, E.D., 2016. Hosed vs. unhosed: interruptions of the Atlantic Meridional Overturning Circulation in a global coupled model, with and without freshwater forcing. Clim. Past 12 (Aug.), 1663–1679.

Buiron, D., Stenni, B., Chappellaz, J., Landais, A., Baumgartner, M., Bonazza, M., Capron, E., Frezzotti, M., Kageyama, M., Lemieux-Dudon, B., Masson-Delmotte, V., Parrenin, F., Schilt, A., Selmo, E., Severi, M., Swingedouw, D., Udisti, R., 2012. Regional imprints of millennial variability during the MIS 3 period around Antarctica. Quat. Sci. Rev. 48 (Aug.), 99–112.

Buizert, C., Gkinis, V., Severinghaus, J.P., He, F., Lecavalier, B.S., Kindler, P., Leuenberger, M., Carlson, A.E., Vinther, B., Masson-Delmotte, V., White, J.W.C., Liu, Z., Otto-Bliesner, B., Brook, E.J., 2014. Greenland temperature response to climate forcing during the last deglaciation. Science 345 (Sept.), 1177–1180.

Buizert, C., Keisling, B.A., Box, J.E., He, F., Carlson, A.E., Sinclair, G., DeConto, R.M., 2018. Greenland-wide seasonal temperatures during the last deglaciation. Geophys. Res. Lett. 45, 1905–1914, 2017GL075601.

Buizert, C., Schmittner, A., 2015. Southern Ocean control of glacial AMOC stability and Dansgaard-Oeschger interstadial duration. Paleoceanography 30 (12), 1595–1612, 2015PA002795.

Cabré, A., Marinov, I., Gnanadesikan, A., 2017. Global atmospheric teleconnections and multidecadal climate oscillations driven by Southern Ocean convection. J. Clim. 30 (Oct.), 8107–8126.

Ceppi, P., Hwang, Y.-T., Liu, X., Frierson, D.M.W., Hartmann, D.L., 2013. The relationship between the ITCZ and the Southern Hemispheric eddy-driven jet. J. Geophys. Res. Atmos. 118 (June), 5136–5146.

Chase, B.M., Boom, A., Carr, A.S., Carr, M., Chevalier, M., Meadows, M.E., Pedro, J.B., Stager, J.C., Reimer, P.J., 2015. Evolving southwest African response to abrupt deglacial North Atlantic climate change events. Quat. Sci. Rev. 121 (Suppl. C), 132–136.

Cheng, H., Sinha, A., Cruz, F.W., Wang, X., Edwards, R.L., D'Horta, F.M., Ribas, C.C., Vuille, M., Stott, L.D., Auler, A.S., 2013. Climate change patterns in Amazonia and biodiversity. Nat. Commun. 4 (Jan.), 1411.

Cheng, W., Bitz, C.M., Chiang, J.C.H., 2007. Adjustment of the global climate to an abrupt slowdown of the Atlantic Meridional Overturning Circulation. Wash. D.C. Am. Geophys. Union Geophys. Monogr. Ser. 173, 295–313.

Chiang, J.C.H., Bitz, C.M., 2005. Influence of high latitude ice cover on the marine Intertropical Convergence Zone. Clim. Dyn. 25 (Oct.), 477–496.

Chiang, J.C.H., Cheng, W., Bitz, C.M., 2008. Fast teleconnections to the tropical Atlantic sector from Atlantic thermohaline adjustment. Geophys. Res. Lett. 35 (7), L07704.

Clement, A.C., Peterson, L.C., 2008. Mechanisms of abrupt climate change of the last glacial period. Rev. Geophys. 46 (4), RG4002.

Collins, W.D., Bitz, C.M., Blackmon, M.L., Bonan, G.B., Bretherton, C.S., Carton, J.A., Chang, P., Doney, S.C., Hack, J.J., Henderson, T.B., Kiehl, J.T., Large, W.G., McKenna, D.S., Santer, B.D., Smith, R.D., 2006. The Community Climate System Model Version 3 (CCSM3). J. Clim. 19, 2122.

Cox, M.D., 1989. An idealized model of the world ocean. Part I: the global-scale

water masses. J. Phys. Oceanogr. 19 (11), 1730–1752.
Croll, J., 1870. On ocean currents. London Edinburgh Dublin Philos. Mag. J. Sci. (Fourth Series) 39, 81–106.
Crowley, T., 1992. North Atlantic deepwater cools the southern hemisphere. Paleoceanography 7 (4), 489–497.
Cuffey, K.M., Clow, G.D., Steig, E.J., Buizert, C., Fudge, T.J., Koutnik, M., Waddington, E.D., Alley, R.B., Severinghaus, J.P., 2016. Deglacial temperature history of West Antarctica. Proc. Natl. Acad. Sci. 113 (50), 14249–14254.
Curry, W.B., Oppo, D.W., 1997. Synchronous, high-frequency oscillations in tropical sea surface temperatures and North Atlantic deep water production during the last glacial cycle. Paleoceanography 12 (1), 1–14.
Ding, Q., Steig, E.J., Battisti, D.S., Küttel, M., 2011. Winter warming in West Antarctica caused by central tropical Pacific warming. Nat. Geosci. 4 (June), 398–403.
Dokken, T.M., Nisancioglu, K.H., Li, C., Battisti, D.S., Kissel, C., 2013. Dansgaard-Oeschger cycles: interactions between ocean and sea ice intrinsic to the Nordic seas. Paleoceanography 28 (Sept.), 491–502.
Eden, C., Jochum, M., Danabasoglu, G., 2009. Effects of different closures for thickness diffusivity. Ocean. Modell. 26, 47–59.
EPICA Community Members, 2006. One-to-one coupling of glacial climate variability in Greenland and Antarctica. Nature 444 (Nov.), 195–198.
Ezat, M.M., Rasmussen, T.L., Groeneveld, J., 2014. Persistent intermediate water warming during cold stadials in the southeastern Nordic seas during the past 65 k.y. Geology 42 (Aug.), 663–666.
Farneti, R., Vallis, G.K., 2013. Meridional energy transport in the coupled atmosphere-ocean system: compensation and partitioning. J. Clim. 26 (Sept.), 7151–7166.
Frierson, D.M.W., Hwang, Y.-T., Fučkar, N.S., Seager, R., Kang, S.M., Donohoe, A., Maroon, E.A., Liu, X., Battisti, D.S., 2013. Contribution of ocean overturning circulation to tropical rainfall peak in the Northern Hemisphere. Nat. Geosci. 6 (Nov.), 940–944.
Galbraith, E.D., Merlis, T.M., Palter, J.B., 2016. Destabilization of glacial climate by the radiative impact of Atlantic Meridional Overturning Circulation disruptions. Geophys. Res. Lett. 43 (Aug.), 8214–8221.
Ganachaud, A., Wunsch, C., 2000. Improved estimates of global ocean circulation, heat transport and mixing from hydrographic data. Nature 408 (Nov.), 453–457.
Ganopolski, A., Rahmstorf, S., 2001. Rapid changes of glacial climate simulated in a coupled climate model. Nature 409 (Jan.), 153–158.
Gent, P.R., McWilliams, J.C., 1990. Isopycnal mixing in ocean circulation models. J. Phys. Oceanogr. 20 (Jan.), 150–160.
Gottschalk, J., Skinner, L.C., Misra, S., Waelbroeck, C., Menviel, L., Timmermann, A., 2015. Abrupt changes in the southern extent of north Atlantic deep water during Dansgaard-Oeschger events. Nat. Geosci. 8 (Dec.), 950–954.
Gupta, A.S., England, M.H., 2007. Coupled ocean atmosphere feedback in the Southern Annular Mode. J. Clim. 20, 3677.
Hartmann, D., 2016. Global Physical Climatology, Second Edition. Elsevier, Amsterdam, Netherlands, 485pp.
He, F., 2011. Simulating Transient Climate Evolution of the Last Deglaciation. PhD Thesis, University of Wisconsin-Maddison, 185pp.
He, F., Shakun, J.D., Clark, P.U., Carlson, A.E., Liu, Z., Otto-Bliesner, B.L., Kutzbach, J.E., 2013. Northern Hemisphere forcing of Southern Hemisphere climate during the last deglaciation. Nature 494 (Feb.), 81–85.
Headly, M.A., Severinghaus, J.P., 2007. A method to measure Kr/N_2 ratios in air bubbles trapped in ice cores and its application in reconstructing past mean ocean temperature. J. Geophys. Res. Atmos. 112 (Oct.), D19105.
Henry, L.G., McManus, J.F., Curry, W.B., Roberts, N.L., Piotrowski, A.M., Keigwin, L.D., 2016. North Atlantic ocean circulation and abrupt climate change during the last glaciation. Science 353 (July), 470–474.
Huang, R.X., Cane, M.A., Naik, N., Goodman, P., 2000. Global adjustment of the thermocline in response to deepwater formation. Geophys. Res. Lett. 27 (Mar.), 759–762.
Huber, C., Leuenberger, M., Spahni, R., Flückiger, J., Schwander, J., Stocker, T.F., Johnsen, S., Landais, A., Jouzel, J., 2006. Isotope calibrated Greenland temperature record over Marine Isotope Stage 3 and its relation to CH_4. Earth Planet. Sci. Lett. 243 (Mar.), 504–519.
Huybers, P., 2004. Comments on `Coupling of the hemispheres in observations and simulations of glacial climate change' by A. Schmittner, O.A. Saenko, and A.J. Weaver. Quat. Sci. Rev. 23 (Jan.), 207–210.
Jochum, M., Eden, C., 2015. The connection between Southern Ocean winds, the Atlantic Meridional Overturning Circulation, and Indo-Pacific upwelling. J. Clim. 28 (Dec.), 9250–9257.
Jochum, M., Malanotte-Rizzoli, P., 2001. Influence of the Meridional Overturning Circulation on Tropical Subtropical pathways. J. Phys. Oceanogr. 31 (May), 1313–1323.
Jochum, M., Danabasoglu, G., Holland, M., Kwon, Y.-O., Large, W.G., 2008. Ocean viscosity and climate. J. Geophys. Res. (Oceans) 113 (June), C06017.
Johnson, H.L., Marshall, D.P., 2002. A theory for the surface Atlantic response to thermohaline variability. J. Phys. Oceanogr. 32 (Apr.), 1121–1132.
Jouzel, J., Alley, R.B., Cuffey, K.M., Dansgaard, W., Grootes, P., Hoffmann, G., Johnsen, S.J., Koster, R.D., Peel, D., Shuman, C.A., Stievenard, M., Stuiver, M., White, J., 1997. Validity of the temperature reconstruction from water isotopes in ice cores. J. Geophys. Res. Oceans 102 (C12), 26471–26487.
Kageyama, M., Merkel, U., Otto-Bliesner, B., Prange, M., Abe-Ouchi, A., Lohmann, G., Ohgaito, R., Roche, D.M., Singarayer, J., Swingedouw, D., Zhang, X., 2013. Climatic impacts of fresh water hosing under Last Glacial Maximum conditions: a multi-model study. Clim. Past 9 (Apr), 935–953.
Kang, S.M., Held, I.M., Frierson, D.M.W., Zhao, M., 2008. The response of the ITCZ to extratropical thermal forcing: idealized slab-ocean experiments with a GCM. J. Clim. 21, 3521–3532.
Kawase, M., 1987. Establishment of deep ocean circulation driven by deep-water production. J. Phys. Oceanogr. 17, 2294–2317.
Kim, J.-H., Schneider, R.R., Mulitza, S., Müller, P.J., 2003. Reconstruction of SE trade-wind intensity based on sea-surface temperature gradients in the Southeast Atlantic over the last 25 kyr. Geophys. Res. Lett. 30 (Nov.), 2144.
Kindler, P., Guillevic, M., Baumgartner, M., Schwander, J., Landais, A., Leuenberger, M., Spahni, R., Capron, E., Chappellaz, J., 2014. Temperature reconstruction from 10 to 120 kyr b2k from the NGRIP ice core. Clim. Past 10 (Apr.), 887–902.
Kissel, C., Laj, C., Piotrowski, A.M., Goldstein, S.L., Hemming, S.R., 2008. Millennial-scale propagation of Atlantic deep waters to the glacial Southern Ocean. Paleoceanography 23 (June), PA2102.
Kleppin, H., Jochum, M., Otto-Bliesner, B., Shields, C.A., Yeager, S., 2015. Stochastic atmospheric forcing as a cause of Greenland climate transitions. J. Clim. 28 (Oct.), 7741–7763.
Knutti, R., Fluckiger, J., Stocker, T.F., Timmermann, A., 2004. Strong hemispheric coupling of glacial climate through freshwater discharge and ocean circulation. Nature 430, 851–856.
Kuhlbrodt, T., Griesel, A., Montoya, M., Levermann, A., Hofmann, M., Rahmstorf, S., 2007. On the driving processes of the Atlantic Meridional Overturning Circulation. Rev. Geophys. 45 (June), RG2001.
Lamy, F., Arz, H.W., Kilian, R., Lange, C.B., Lembke-Jene, L., Wengler, M., Kaiser, J., Baeza-Urrea, O., Hall, I.R., Harada, N., Tiedemann, R., 2015. Glacial reduction and millennial-scale variations in Drake Passage throughflow. Proc. Natl. Acad. Sci. 112 (Nov.), 13496–13501.
Lamy, F., Kaiser, JRME, Arz, H.W., Hebbeln, D., Ninnemann, U., Timm, O., Timmermann, A., Toggweiler, J.R., 2007. Modulation of the bipolar seesaw in the Southeast Pacific during Termination 1. Earth Planet. Sci. Lett. 259 (34), 400–413.
Landais, A., Masson-Delmotte, V., Stenni, B., Selmo, E., Roche, D.M., Jouzel, J., Lambert, F., Guillevic, M., Bazin, L., Arzel, O., Vinther, B., Gkinis, V., Popp, T., 2015. A review of the bipolar seesaw from synchronized and high resolution ice core water stable isotope records from Greenland and East Antarctica. Quat. Sci. Rev. 114, 18–32.
Lee, S., Kim, H.-K., 2003. The dynamical relationship between subtropical and eddy-driven jets. J. Atmos. Sci. 60 (June), 1490–1503.
Lee, S.-Y., Chiang, J.C.H., Matsumoto, K., Tokos, K.S., 2011. Southern Ocean wind response to North Atlantic cooling and the rise in atmospheric CO_2: modeling perspective and paleoceanographic implications. Paleoceanography 26 (Mar.), PA1214.
Levitus, S., Antonov, J.I., Boyer, T.P., Baranova, O.K., Garcia, H.E., Locarnini, R.A., Mishonov, A.V., Reagan, J.R., Seidov, D., Yarosh, E.S., Zweng, M.M., 2012. World ocean heat content and thermosteric sea level change (0-2000 m), 1955-2010. Geophys. Res. Lett. 39 (May), L10603.
Liu, Z., Philander, S.G.H., Pacanowski, R.C., 1994. A GCM study of tropical–subtropical upper-ocean water exchange. J. Phys. Oceanogr. 24 (12), 2606–2623.
Liu, Z., Otto-Bliesner, B.L., He, F., Brady, E.C., Tomas, R., Clark, P.U., Carlson, A.E., Lynch-Stieglitz, J., Curry, W., Brook, E., Erickson, D., Jacob, R., Kutzbach, J., Cheng, J., 2009. Transient simulation of last deglaciation with a new mechanism for Bølling-Allerød warming. Science 325 (July), 310.
Liu, Z., Philander, S.G.H., 1995. How different wind stress patterns affect the tropical-subtropical circulations of the upper ocean. J. Phys. Oceanogr. 25 (4), 449–462.
Lübbecke, J.F., 2013. Tropical Atlantic warm events. Nat. Geosci. 6 (Jan.), 22–23.
Luyten, J.R., Pedlosky, J., Stommel, H., 1983. The ventilated thermocline. J. Phys. Oceanogr. 13 (Feb.), 292–309.
Lynch-Stieglitz, J., 2017. The Atlantic Meridional Overturning Circulation and abrupt climate change. Annu. Rev. Mar. Sci. 9 (Jan.), 83–104.
Marcott, S.A., Clark, P.U., Padman, L., Klinkhammer, G.P., Springer, S.R., Liu, Z., Otto-Bliesner, B.L., Carlson, A.E., Ungerer, A., Padman, J., He, F., Cheng, J., Schmittner, A., 2011. Ice-shelf collapse from subsurface warming as a trigger for Heinrich events. Proc. Natl. Acad. Sci. 108 (Aug.), 13415–13419.
Markle, B.R., Steig, E.J., Buizert, C., Schoenemann, S.W., Bitz, C.M., Fudge, T.J., Pedro, J.B., Ding, Q., Jones, T.R., White, J.W.C., Sowers, T., 2017. Global atmospheric teleconnections during Dansgaard-Oeschger events. Nat. Geosci. 10 (Jan.), 36–40.
Marshall, J., Speer, K., 2012. Closure of the meridional overturning circulation through Southern Ocean upwelling. Nat. Geosci. 5, 171–180.
Martin, T., Park, W., Latif, M., 2015. Southern Ocean forcing of the north Atlantic at multi-centennial time scales in the Kiel Climate Model. Deep Sea Res. Part II Top. Stud. Oceanogr. 114 (Apr.), 39–48.
McDougall, T.J., Church, J.A., 1986. Pitfalls with the numerical representation of isopycnal diapycnal mixing. J. Phys. Oceanogr. 16 (1), 196–199.
Menviel, L., Spence, P., England, M.H., 2015. Contribution of enhanced Antarctic Bottom Water formation to Antarctic warm events and millennial-scale atmospheric CO_2 increase. Earth Planet. Sci. Lett. 413 (Mar.), 37–50.
Mix, A.C., Ruddiman, W.F., McIntyre, A., 1986. Late Quaternary paleoceanography of the Tropical Atlantic, 1: spatial variability of annual mean sea-surface temperatures, 0-20,000 years B.P. Paleoceanography 1 (1), 43–66.
Moreno, P.I., Villa-Martnez, R., Crdenas, M.L., Sagredo, E.A., 2012. Deglacial changes of the southern margin of the southern westerly winds revealed by terrestrial records from SW Patagonia (52S). Quat. Sci. Rev. 41 (Suppl. C), 1–21.

Morgan, V., Delmotte, M., van Ommen, T., Jouzel, J., Chappellaz, J., Woon, S., Masson-Delmotte, V., Raynaud, D., 2002. Relative timing of deglacial climate events in Antarctica and Greenland. Science 297 (Sept.), 1862–1864.
Mosblech, N.A.S., Bush, M.B., Gosling, W.D., Hodell, D., Thomas, L., van Calsteren, P., Correa-Metrio, A., Valencia, B.G., Curtis, J., van Woesik, R., 2012. North Atlantic forcing of Amazonian precipitation during the last ice age. Nat. Geosci. 5 (Nov.), 817–820.
Munday, D.R., Johnson, H.L., Marshall, D.P., 2013. Eddy saturation of equilibrated circumpolar currents. J. Phys. Oceanogr. 43 (Mar.), 507–532.
Munk, W., Wunsch, C., 1998. Abyssal Recipies II: energetics of tidal and wind mixing. Deep Sea Res. I 45, 1977–2010.
Nelson, G., Hutchings, L., 1983. The Benguela upwelling area. Prog. Oceanogr. 12, 333–356.
North Greenland Ice Core Project members, 2004. High-resolution record of Northern Hemisphere climate extending into the last interglacial period. Nature 431, 147–151.
Otto-Bliesner, B.L., Brady, E.C., 2010. The sensitivity of the climate response to the magnitude and location of freshwater forcing: last glacial maximum experiments. Quat. Sci. Rev. 29 (1), 56–73 (Climate of the Last Million Years: New Insights from EPICA and Other Records).
Parrenin, F., Masson-Delmotte, V., Köhler, P., Raynaud, D., Paillard, D., Schwander, J., Barbante, C., Landais, A., Wegner, A., Jouzel, J., 2013. Synchronous change of atmospheric CO_2 and Antarctic temperature during the last deglacial warming. Science 339 (6123), 1060–1063.
Pedro, J.B., van Ommen, T.D., Rasmussen, S.O., Morgan, V.I., Chappellaz, J., Moy, A.D., Masson-Delmotte, V., Delmotte, M., 2011. The last deglaciation: timing the bipolar seesaw. Clim. Past 7 (June), 671–683.
Pedro, J.B., Martin, T., Steig, E.J., Jochum, M., Park, W., Rasmussen, S.O., 2016a. Southern Ocean deep convection as a driver of Antarctic warming events. Geophys. Res. Lett. 43 (mar), 2192–2199.
Pedro, J.B., Bostock, H.C., Bitz, C.M., He, F., Vandergoes, M.J., Steig, E.J., Chase, B.M., Krause, C.E., Rasmussen, S.O., Markle, B.R., Cortese, G., 2016b. The spatial extent and dynamics of the Antarctic Cold Reversal. Nat. Geosci. 9 (Jan.), 51–55.
Peltier, W.R., Vettoretti, G., 2014. Dansgaard-Oeschger oscillations predicted in a comprehensive model of glacial climate: a kicked salt oscillator in the Atlantic. Geophys. Res. Lett. 41 (20), 7306–7313, 2014GL061413.
Peterson, L.C., Haug, G.H., Hughen, K.A., Röhl, U., 2000. Rapid changes in the hydrologic cycle of the tropical Atlantic during the last glacial. Science 290 (Dec.), 1947–1951.
Piotrowski, A.M., Goldstein, S.L., Hemming, S.R., Fairbanks, R.G., 2005. Temporal relationships of carbon cycling and ocean circulation at glacial boundaries. Science 307 (Mar.), 1933–1938.
Previdi, M., Smith, K.L., Polvani, L.M., 2013. The Antarctic atmospheric energy budget. Part I: climatology and intraseasonal-to-interannual variability. J. Clim. 26 (17), 6406–6418.
Putnam, A.E., Denton, G.H., Schaefer, J.M., Barrell, D.J.A., Andersen, B.G., Finkel, R.C., Schwartz, R., Doughty, A.M., Kaplan, M.R., Schlüchter, C., 2010. Glacier advance in southern middle-latitudes during the Antarctic Cold Reversal. Nat. Geosci. 3 (Oct.), 700–704.
Raisbeck, G.M., Cauquoin, A., Jouzel, J., Landais, A., Petit, J.-R., Lipenkov, V.Y., Beer, J., Synal, H.-A., Oerter, H., Johnsen, S.J., Steffensen, J.P., Svensson, A., Yiou, F., 2017. An improved north-south synchronization of ice core records around the 41 kyr ^{10}Be peak. Clim. Past 13 (Mar.), 217–229.
Rasmussen, S.O., Bigler, M., Blockley, S.P., Blunier, T., Buchardt, S.L., Clausen, H.B., Cvijanovic, I., Dahl-Jensen, D., Johnsen, S.J., Fischer, H., Gkinis, V., Guillevic, M., Hoek, W.Z., Lowe, J.J., Pedro, J.B., Popp, T., Seierstad, I.K., Steffensen, J.P., Svensson, A.M., Vallelonga, P., Vinther, B.M., Walker, M.J.C., Wheatley, J.J., Winstrup, M., 2014. A stratigraphic framework for abrupt climatic changes during the Last Glacial period based on three synchronized Greenland ice-core records: refining and extending the *INTIMATE* event stratigraphy. Quat. Sci. Rev. 106, 14–28.
Rasmussen, T.L., Thomsen, E., Moros, M., 2016. North Atlantic warming during Dansgaard-Oeschger events synchronous with Antarctic warming and out-of-phase with Greenland climate. Sci. Rep. 6 (Feb.), 20535.
Rintoul, S.R., Naveira Garabato, A.C., 2013. Dynamics of the Southern Ocean circulation. In: Siedler, G. (Ed.), Ocean Circulation and Climate: a 21st Century Perspective. Int. Geophys, vol. 103. Academic Press, pp. 471–492.
Ruddiman, W.F., McIntyre, A., 1981. The mode and mechanism of the last deglaciation: oceanic evidence. Quat. Res. 16 (Sept.), 125–134.
Sachs, J.P., Lehman, S.J., 1999. Subtropical North Atlantic temperatures 60,000 to 30,000 years ago. Science 286 (5440), 756–759.
Schmittner, A., Saenko, O.A., Weaver, A.J., 2003. Coupling of the hemispheres in observations and simulations of glacial climate change. Quat. Sci. Rev. 22 (Mar.), 659–671.
Seager, R., Battisti, D., 2007. Challenges to our understanding of the general circulation: Abrupt climate change. Princeton University Press, pp. 332–372. Chap. 11.
Seidov, D., Maslin, M., 2001. Atlantic ocean heat piracy and the bipolar climate seesaw during Heinrich and Dansgaard-Oeschger events. J. Quat. Sci. 16 (May), 321–328.
Severinghaus, J.P., Sowers, T., Brook, E.J., Alley, R.B., Bender, M.L., 1998. Timing of abrupt climate change at the end of the Younger Dryas interval from thermally fractionated gases in polar ice. Nature 391 (Jan.), 141–146.
Shackleton, N.J., Hall, M.A., Vincent, E., 2000. Phase relationships between millennial-scale events 64,000-24,000 years ago. Paleoceanography 15 (Dec.), 565–569.
Shaffrey, L., Sutton, R., 2004. The interannual variability of energy transports within and over the Atlantic Ocean in a coupled climate model. J. Clim. 17 (Apr.), 1433–1448.
Sime, L.C., Hodgson, D., Bracegirdle, T.J., Allen, C., Perren, B., Roberts, S., de Boer, A.M., 2016. Sea ice led to poleward-shifted winds at the Last Glacial Maximum: the influence of state dependency on CMIP5 and PMIP3 models. Clim. Past 12 (Dec.), 2241–2253.
Staten, P.W., Reichler, T., 2014. On the ratio between shifts in the eddy-driven jet and the Hadley cell edge. Clim. Dyn. 42 (Mar.), 1229–1242.
Steffensen, J.P., Andersen, K.K., Bigler, M., Clausen, H.B., Dahl-Jensen, D., Fischer, H., Goto-Azuma, K., Hansson, M., Johnsen, S.J., Jouzel, J., Masson-Delmotte, V., Popp, T., Rasmussen, S.O., Röthlisberger, R., Ruth, U., Stauffer, B., Siggaard-Andersen, M.-L., Sveinbjörnsdóttir, Á.E., Svensson, A., White, J.W.C., 2008. High-resolution Greenland ice core data show abrupt climate change happens in few years. Science 321 (aug), 680.
Steig, E.J., Alley, R.B., 2002. Phase relationships between Antarctic and Greenland climate records. Ann. Glaciol. 35 (Jan.), 451–456.
Stenni, B., Buiron, D., Frezzotti, M., Albani, S., Barbante, C., Bard, E., Barnola, J.M., Baroni, M., Baumgartner, M., Bonazza, M., Capron, E., Castellano, E., Chappellaz, J., Delmonte, B., Falourd, S., Genoni, L., Iacumin, P., Jouzel, J., Kipfstuhl, S., Landais, A., Lemieux-Dudon, B., Maggi, V., Masson-Delmotte, V., Mazzola, C., Minster, B., Montagnat, M., Mulvaney, R., Narcisi, B., Oerter, H., Parrenin, F., Petit, J.R., Ritz, C., Scarchilli, C., Schilt, A., Schüpbach, S., Schwander, J., Selmo, E., Severi, M., Stocker, T.F., Udisti, R., 2011. Expression of the bipolar see-saw in Antarctic climate records during the last deglaciation. Nat. Geosci. 4 (Jan.), 46–49.
Stocker, T.F., Johnsen, S.J., 2003. A minimum thermodynamic model for the bipolar seesaw. Paleoceanography 18 (Nov.), 11–1.
Stocker, T.F., Mysak, L.A., Wright, D.G., 1992. A zonally averaged, coupled ocean-atmosphere model for paleoclimate studies. J. Clim. 5 (8), 773–797.
Stocker, T.F., Timmermann, A., Renold, M., Timm, O., 2007. Effects of salt compensation on the climate model response in simulations of large changes of the Atlantic Meridional Overturning Circulation. J. Clim. 20 (24), 5912–5928.
Stommel, H., 1961. Thermohaline convection with two stable regimes of flow. Tellus 13 (2), 224–230.
Stouffer, R.J., Seidov, D., Haupt, B.J., 2007. Climate response to external sources of freshwater: north Atlantic versus the Southern Ocean. J. Clim. 20, 436.
Swingedouw, D., Fichefet, T., Goosse, H., Loutre, M.F., 2009. Impact of transient freshwater releases in the Southern Ocean on the AMOC and climate. Clim. Dyn. 33 (Aug.), 365–381.
Talley, L.D., 2013. Closure of the global overturning circulation through the Indian, Pacific, and Southern Oceans: schematics and transports. Oceanography 26, 80–97.
Thomas, E.R., Wolff, E.W., Mulvaney, R., Johnsen, S.J., Steffensen, J.P., Arrowsmith, C., 2009. Anatomy of a Dansgaard-Oeschger warming transition: high-resolution analysis of the North Greenland Ice Core Project ice core. J. Geophys. Res. Atmos. 114 (Apr.), D08102.
Tierney, J.E., Russell, J.M., Huang, Y., Damsté, J.S.S., Hopmans, E.C., Cohen, A.S., 2008. Northern hemisphere controls on tropical southeast African climate during the past 60,000 years. Science 322 (Oct.), 252.
Timmermann, A., Menviel, L., Okumura, Y., Schilla, A., Merkel, U., Timm, O., Hu, A., Otto-Bliesner, B., Schulz, M., 2010. Towards a quantitative understanding of millennial-scale Antarctic warming events. Quat. Sci. Rev. 29 (Jan.), 74–85.
Toggweiler, J.R., Samuels, B., 1995. Effect of Drake Passage on the global thermohaline circulation. Deep Sea Res. Part I Oceanogr. Res. Pap. 42 (4), 477–500.
Trenberth, K.E., Caron, J.M., 2001. Estimates of meridional atmosphere and ocean heat transports. J. Clim. 14 (Aug.), 3433–3443.
Trenberth, K.E., Fasullo, J.T., 2017. Atlantic meridional heat transports computed from balancing Earth's energy locally. Geophys. Res. Lett. 44 (Feb.), 1919–1927.
Vellinga, M., Wood, R.A., 2002. Global climatic impacts of a collapse of the Atlantic thermohaline circulation. Clim. Change 54, 251–267.
Veres, D., Bazin, L., Landais, A., Toyé Mahamadou Kele, H., Lemieux-Dudon, B., Parrenin, F., Martinerie, P., Blayo, E., Blunier, T., Capron, E., Chappellaz, J., Rasmussen, S.O., Severi, M., Svensson, A., Vinther, B., Wolff, E.W., 2013. The Antarctic ice core chronology (AICC2012): an optimized multi-parameter and multi-site dating approach for the last 120 thousand years. Clim. Past 9 (4), 1733–1748.
Vettoretti, G., Peltier, W.R., 2015. Interhemispheric air temperature phase relationships in the nonlinear Dansgaard-Oeschger oscillation. Geophys. Res. Lett. 42 (4), 1180–1189, 2014GL062898.
Vettoretti, G., Peltier, W.R., 2018. Fast physics and slow physics in the nonlinear Dansgaard-Oeschger relaxation oscillation. J. Clim. https://doi.org/10.1175/JCLI-D-17-0559.1.
WAIS Divide Project Members, 2015. Precise interpolar phasing of abrupt climate change during the last ice age. Nature 520, 661–665.
Wang, Y.J., Cheng, H., Edwards, R.L., An, Z.S., Wu, J.Y., Shen, C.-C., Dorale, J.A., 2001. A high-resolution absolute-dated late Pleistocene monsoon record from Hulu Cave, China. Science 294 (Dec.), 2345–2348.
Weldeab, S., Friedrich, T., Timmermann, A., Schneider, R.R., 2016. Strong middepth warming and weak radiocarbon imprints in the equatorial Atlantic during Heinrich 1 and Younger Dryas. Paleoceanography 31 (8), 1070–1082, 2016PA002957.
Wunsch, C., 2006. Abrupt climate change: an alternative view. Quat. Res. 65 (Mar.), 191–203.

Xie, S.-P., Carton, J.A., 2004. Tropical Atlantic variability: patterns, mechanisms, and impacts. Wash. D.C. Am. Geophys. Union Geophys. Monogr. Ser. 147, 121–142.
Zhang, R., Delworth, T.L., 2005. Simulated tropical response to a substantial weakening of the Atlantic thermohaline circulation. J. Clim. 18 (June), 1853–1860.
Zhang, R.-H., Liu, Z., 1999. Decadal thermocline variability in the North Pacific Ocean: two pathways around the subtropical gyre. J. Clim. 12 (11), 3273–3296.
Zhang, X., Lohmann, G., Knorr, G., Purcell, C., 2014. Abrupt glacial climate shifts controlled by ice sheet changes. Nature 512 (Aug.), 290–294.
Zhang, X., Knorr, G., Lohmann, G., Barker, S., 2017. Abrupt North Atlantic circulation changes in response to gradual CO_2 forcing in a glacial climate state. Nat. Geosci. 10 (July), 518–523.